Charged and magnetized particles motion in the field of generic singular black holes governed by general relativity coupled to nonlinear electrodynamics

Jaroslav Vrba,[1,*] Ahmadjon Abdujabbarov,[2–6,†] Martin Kološ,[1,‡] Bobomurat Ahmedov,[2,3,4,§] Zdeněk Stuchlík,[1,‖] and Javlon Rayimbaev[2,4,6,¶]

[1]*Research Centre for Theoretical Physics and Astrophysics, Institute of Physics in Opava, Silesian University in Opava, Bezručovo náměstí 13, CZ-74601 Opava, Czech Republic*
[2]*Ulugh Beg Astronomical Institute, Astronomicheskaya 33, Tashkent 100052, Uzbekistan*
[3]*Tashkent Institute of Irrigation and Agricultural Mechanization Engineers, Kori Niyoziy, 39, Tashkent 100000, Uzbekistan*
[4]*National University of Uzbekistan, Tashkent 100174, Uzbekistan*
[5]*Shanghai Astronomical Observatory, 80 Nandan Road, Shanghai 200030, China*
[6]*Institute of Nuclear Physics, Tashkent 100214, Uzbekistan*

(Received 16 April 2020; revised manuscript received 18 May 2020; accepted 1 June 2020; published 22 June 2020)

We study spherically symmetric magnetically charged generic singular black hole solutions of general relativity coupled to nonlinear electrodynamics. For characteristic values of the generic spacetime parameters and the parameter characterizing the ratio of the gravitational and electromagnetic forces acting on an electrically charged particle we study the circular orbits and related epicyclic motion and its frequencies. We demonstrate that the equatorial circular orbits are forbidden in such situations, but off-equatorial circular orbits are possible. We give dependence of the stable circular orbit on the spacetime parameters and intensity of the electromagnetic interaction of the charged particles with magnetically charged black holes. We study the possible resonance phenomena of the epicyclic frequencies and the orbital frequency of the electrically charged particles in order to fit the data of the twin high-frequency quasiperiodic oscillations of x rays observed in microquasars. Moreover, the dynamics of magnetized particles around the magnetically charged generic black hole have also been explored and it is shown that as increasing magnetic charge and magnetic moment parameters, the innermost stable circular orbit (ISCO) radius decreases and disappears at some value of the magnetic moment parameter, inversely proportional to the magnetic charge of black hole. As an astrophysical application we treated the magnetar PSR J1745–2900 orbiting around Sagittarius (Sgr) A* as a magnetized particle and showed that the magnetic charge of black hole can mimic black hole spin up to $a/M = 0.865694$ at $\nu = 2$, and the spin parameter can mimic the magnetic charge parameter up to $q/M = 0.578575$ at $\nu = 1$, providing exactly the same value of the ISCO radius. Finally, we predict that no magnetar with the surface magnetic field of the order of 10^{14}–10^{15} G can follow stable orbits, but it is possible to observe ordinary neutron stars as recycled radio pulsars in the close environment of Sgr A*.

DOI: 10.1103/PhysRevD.101.124039

I. INTRODUCTION

One of the fundamental problems of classical theories of gravity, particularly of general relativity (GR), is the presence of physical singularity at the center of black holes [1]. The problem is even stronger, if the physical singularity is not hidden behind the event horizon, i.e., in the case of the so-called naked singularities. The Kerr (Kerr-Newman) geometry describing the most general axially symmetric black holes can describe a rotating Kerr (Kerr-Newman) naked singularity if its dimensionless rotation parameter $\frac{J^2}{M^2} > 1$ (or in addition with its electric charge Q there is condition $\frac{J^2}{M^2} + \frac{Q^2}{M^2} > 1$) [2–4]; the rotating singularity could be avoided in the framework of super-spinars related to the string theory and implying a variety of extraordinary physical phenomena [5–10]. A spherical Reissner-Nordstrom naked singularity exists if $\frac{Q^2}{M^2} > 1$ [11]. A similar situation occurs in the case of the presence of the cosmological constant [12–17]. On the other hand, a

*jaroslav.vrba@physics.slu.cz
†ahmadjon@astrin.uz
‡martin.kolos@physics.slu.cz
§ahmedov@astrin.uz
‖zdenek.stuchlik@physics.slu.cz
¶javlon@astrin.uz

realistic astrophysical scenario of spherically symmetric gravitational collapse can also cause formation of a naked singularity [18–21]. Several ways of avoiding the singularity problem have been suggested by different authors in various ways: conformal gravity models [22–27], quantum corrections [28,29], dark energy star–gravastar models [30–33] and others. Study of the particle motion around black holes in various alternative theories of gravity, or around magnetized black holes, can be found, e.g., in [34–53].

A special way of avoiding physical singularity due to combination of general relativity with a nonlinear electrodynamics (NED) is widely discussed [54–58]. The particle motion in the Bardeen and Ayon-Beato-Garcia backgrounds, of both the black hole and no-horizon type, has been studied in [59,60]. The rotating regular black holes of these types were also considered [57,58]. Properties of the rotating regular black holes have been studied in Ref. [61].

One of the interesting models of NED predicts so-called generic regular black holes [62,63]. The generic regular black holes are generally well defined for magnetically charged cases [63,64]. The class of generic regular black holes contains as subclasses the Bardeen regular black holes, the Hayward regular black holes, and the very important case of the Maxwellian regular black holes giving the proper Maxwell weak field limit of the NED theory that seems to be the only acceptable version of the NED models due to the properties of the optical phenomena related to the Keplerian accretion disks [65–68].

It is of course interesting to study properties of the generic black holes containing the physical singularity and compare the differences to the regular generic black holes. In our preceding paper we have analyzed the structure of the geometry of the singular generic black holes proposed in Ref. [63] and tested the motion of uncharged particles in their field [69]. In the present paper we continue our study considering the charged particle motion around generic singular magnetically charged black holes, concentrating on the off-equatorial circular orbits that are a special signature of the influence of the black hole magnetic charge; we study also the epicyclic motion of charged particles around the off-equatorial circular orbits.

The observationally most important features of the orbital motion of test particles around black holes are frequencies of the geodesic epicyclic oscillations near the innermost stable circular orbit (ISCO) that are close to the observed values of high-frequency quasiperiodic oscillations (HF QPOs) [70–72]. There have been many attempts to model the observed QPOs of the x-ray power density in microquasars, particularly, hot-spot models, disc-seismic models, warped disk models and different types of resonance models [73–76]. Up to now there is no unique mechanism explaining the observed phenomena in all the microquasars [77]. However, modifications due to electromagnetic interaction of orbiting charge particles with magnetized black holes [52,78,79], or oscillating string loops [73,80], enable us to overcome difficulties of HF QPO models based on the geodesic epicyclic motion. Since the astrophysical black holes are surrounded by magnetic fields (stellar, galactic, etc.) this model is well motivated. The magnetic fields around black holes and their effect on charged particle motion and energetic processes have been widely studied in [49,50,81–96] within the framework of general relativity and modified/alternative theories of gravity.

The magnetic field of astrophysical compact object is responsible for observational phenomena of the high energy processes in their close environment that can be used to test the gravity theories in the strong field regime through the study of the charged and magnetized particle motion. The magnetic field structure around black holes immersed in external asymptotically uniform magnetic field was first studied in [81]. The electromagnetic properties and charged particle dynamics around compact gravitational objects have been studied in Refs. [34–36, 45,47–51,53,82–84,87–89,92,97–99]. On the other hand the magnetized particle dynamics around black holes in the presence of external magnetic field have been explored in Refs. [39,90,91,93–95,100–105]. Here we investigate the motion of electrically charged and magnetized particles with nonzero magnetic dipole moment in the gravitational and electromagnetic field of magnetically charged generic black holes in GR coupled to NED.

The paper is organized as follows. We start with the review of the spacetime of the generic black holes governed by general relativity coupled with nonlinear electrodynamics in Sec. II. The charged particle motion around charged black holes is considered in Sec. III. The Sections IV and V are devoted to the study of the charged particle epicyclic motion; its frequencies are used in models of twin HF QPOs and applied for the data obtained in three selected microquasars. Section VI is devoted to magnetized particle motion around magnetically charged black holes in GR coupled to NED. Section VII provides various astrophysical applications for the obtained results, in particular, practical tools to get constrains to black hole parameters through observed particle dynamics in close to environment of SgrA*. We conclude our results in Sec. VIII. Throughout the paper we use the geometrical units where $G = 1 = c$ and spacelike signature $(-1, 1, 1, 1)$. The greek indexes run from 0 to 1.

II. GENERIC BLACK HOLES

We consider the black hole solutions of general relativity coupled to NED with the Lagrangian density introduced in [62] in the form

$$L = \frac{4\mu}{\alpha}\frac{(\alpha F)^{\frac{\nu+3}{4}}}{[1+(\alpha F)^{\frac{\nu}{4}}]^{1+\frac{\mu}{\nu}}},$$

where the Faraday scalar $F = F^{\mu\nu}F_{\mu\nu}$. The parameter $\alpha > 0$ describes the strength of the nonlinear effect, $\mu > 0$ characterizes the degree of nonlinearity and $\nu > 0$ is a free parameter governing character of the electromagnetic field in a concrete solution. In this case the NED theory is well defined for the generic black hole solutions with a magnetic charge when the Faraday scalar $F > 0$ [64,106].

The spherically symmetric generic black hole spacetime metric has a Schwarzschild-like form and in the standard Schwarzschild coordinates its line element has the form [62,106]

$$ds^2 = -\left(1 - \frac{2m(r)}{r}\right)dt^2 + \left(1 - \frac{2m(r)}{r}\right)^{-1}dr^2 + r^2 d\theta^2 + r^2 \sin^2\theta d\phi^2, \tag{1}$$

where the mass function $m(r)$ takes the form [62,63]

$$m(r) = M - \frac{q^3}{\alpha}\left[1 - \frac{r^\mu}{(r^\nu + q^\nu)^{\mu/\nu}}\right]. \tag{2}$$

The magnetic charge related to this solution can be expressed as [61–63]

$$Q_m = \frac{q^2}{\sqrt{2\alpha}}. \tag{3}$$

The parameter q is the integration constant related to the magnetic charge; for our purpose we suppose $q > 0$ [62]. The electromagnetic field potential of the nonrotating magnetically charged generic black holes reads

$$A_\alpha = (0, 0, 0, Q_m \cos\theta). \tag{4}$$

Recall that values of the parameter ν fix the type of the generic black hole; for $\nu = 1$ we have the black holes of the Maxwellian type, for $\nu = 2$ of the Bardeen type, and for $\nu = 3$ of the Hayward type (for details see [67,107]).

The Arnowitt-Deser-Misner (ADM) mass of this solution is defined by

$$M_{\rm ADM} = M + M_{\rm em},$$

with

$$M_{\rm em} = \frac{q^3}{\alpha}$$

being the electromagnetically induced gravitational mass. Note that the generic regular black holes (having no physical singularities at the center $r = 0$) appear when we assume

$$M = M_{\rm em}, \tag{5}$$

with condition $\mu \geq 3$ [62]. Requirement (5) with (2) leads to the mass function governing the regular solutions

$$m(r) = \frac{Mr^\mu}{(r^\nu + q^\nu)^{\mu/\nu}}. \tag{6}$$

Recall that the regular solutions are allowed only for the parameter $\mu \geq 3$.

In our recent study we consider the metric of generic singular magnetically charged black holes (1) with the mass function (2). We do not consider the condition (5) governing the regular (nonsingular) black holes. Due to the studies in [65–67,108] it is obvious that the astrophysically relevant cases occur for the parameter $\nu = 1$ and correspond to the so-called Maxwellian NED black holes. Therefore, we will prefer these spacetimes in our study.

For simplicity we use the dimensionless radius $r/M \to r$, dimensionless charge parameter $q/M \to q$ and dimensionless parameter $\alpha/M^2 \to \alpha$; equivalently, we put $M = 1$.

The position of the black hole horizon is determined by the condition

$$f(r) = -g_{tt}(r) = 1 - \frac{2m(r)}{r} = 0. \tag{7}$$

The existence and behavior of the horizon(s) of the generic black holes and other properties of the generic geometry were studied in [69]. We use results of this paper—we deal with objects having at least one horizon, i.e., black holes.

III. CHARGED PARTICLE MOTION IN THE FIELD OF GENERIC BLACK HOLES

We use the Hamiltonian formalism [109] to describe dynamics of electrically charged particles with charge $q_p \neq 0$ in vicinity of the singular generic magnetically charged black holes. The Hamiltonian H in this case takes the form

$$H = \frac{1}{2}g^{\alpha\beta}(\pi_\alpha - q_p A_\alpha)(\pi_\beta - q_p A_\beta) + \frac{m^2}{2}, \tag{8}$$

while the Hamilton equations of motion read

$$\frac{{\rm d}x^\alpha}{{\rm d}\lambda} = \frac{\partial H}{\partial \pi_\alpha}, \qquad \frac{{\rm d}\pi_\alpha}{{\rm d}\lambda} = -\frac{\partial H}{\partial x^\alpha}, \tag{9}$$

where m is mass of test particle, π_α is canonical four-momentum, q_p is charge of test particle and affine parameter λ is related to the proper time τ by relation $\lambda = \tau/m$.

Due to symmetries of the spherically symmetric generic singular background given by the metric (1) combined with the magnetic monopole field, one can find conserved quantities of the charged particle motion: the specific energy and the specific axial angular momentum—they read, respectively,

$$\mathcal{E} = \frac{E}{m} = -\frac{\pi_t}{m} = -g_{tt}u^t,$$
$$\mathcal{L} = \frac{l}{m} = \frac{\pi_\phi}{m} = g_{\phi\phi}u^\phi + \bar{q}_p A_\phi, \tag{10}$$

where we introduced the specific electric charge of the particle $\bar{q}_p = q_p/m$. Using the conserved quantities (10), the Hamiltonian (8) can be separated into dynamical and potential parts

$$H = H_{\rm dyn} + H_{\rm pot}, \tag{11}$$

where

$$H_{\rm dyn} = \frac{1}{2}(g^{rr}p_r^2 + g^{\theta\theta}p_\theta^2), \tag{12}$$

$$H_{\rm pot} = \frac{m^2}{2}(g^{tt}\mathcal{E}^2 + g^{\phi\phi}(\mathcal{L} - \bar{q}_p A_\phi)^2 + 1). \tag{13}$$

A. Effective potential of the motion and off-equatorial circular orbits

The energetic boundary of the charged particle motion is determined by Eqs. (8) and (10)–(13) due to the conditions of the simultaneous turning points of the radial and latitudinal motion $p_r = p_\theta = 0$ that enable introduction of the effective potential determined by the relation $\mathcal{E} = V_{\rm eff}(r,\theta)$, where the effective potential $V_{\rm eff}(r,\theta)$ is given in the form

$$V_{\rm eff}(r,\theta) \equiv \sqrt{-g_{tt}[g^{\phi\phi}(\mathcal{L} - \bar{q}_p A_\phi)^2 + 1]}. \tag{14}$$

The effective potential describes influence of gravity and central force potentials given by the angular momentum and the electromagnetic potential energy. Positive angular momentum $\mathcal{L} > 0$ corresponds to counterclockwise revolved particle.

Introducing the parameter e governing the relation of the electromagnetic and gravitational interaction

$$e = \frac{q_p Q_m GM}{mc^4}, \tag{15}$$

where we have momentarily introduced for completeness also the gravitational constant G and light velocity c. This parameter e governs the charged particle motion—we distinguish the plus ($e > 0$) and minus ($e < 0$) electromagnetic interactions. The effective potential (14) then can be rewritten as

$$V_{\rm eff}(r,\theta) = \sqrt{\left(1 - \frac{2m(r)}{r}\right)\left[\frac{(\mathcal{L} - e\cos\theta)^2}{r^2\sin^2\theta} + 1\right]}, \tag{16}$$

where $m(r)$ is the mass function (2) governing the singular generic black holes.

The examples of the behavior of the effective potential $V_{\rm eff}(r,\theta)$ are given for the positively and negatively valued parameter e in Fig. 1. Obviously, there exists an important symmetry of the effective potential with respect to the sign of the parameter e—the charged particle dynamics is of the same character if we change the sign of the gravomagnetic parameter e and $\theta \to \pi - \theta$. We can read it directly from the relation giving the effective potential (16) [see the term $(\mathcal{L} - e\cos\theta)^2$]. In Fig. 2 we present the $\theta =$ const sections and the $r =$ const sections of the effective potentials. These figures clearly demonstrate that the effective potential is not symmetric relative to the equatorial plane $\theta = \pi/2$ due to the electromagnetic interaction of the electrically charged particle with the magnetic monopole charge of the black hole, i.e., the existence of e parameter. For neutral particles, this asymmetry disappears. The behavior of the effective potential thus clearly demonstrates very important consequence of the electromagnetic interaction in the case of our

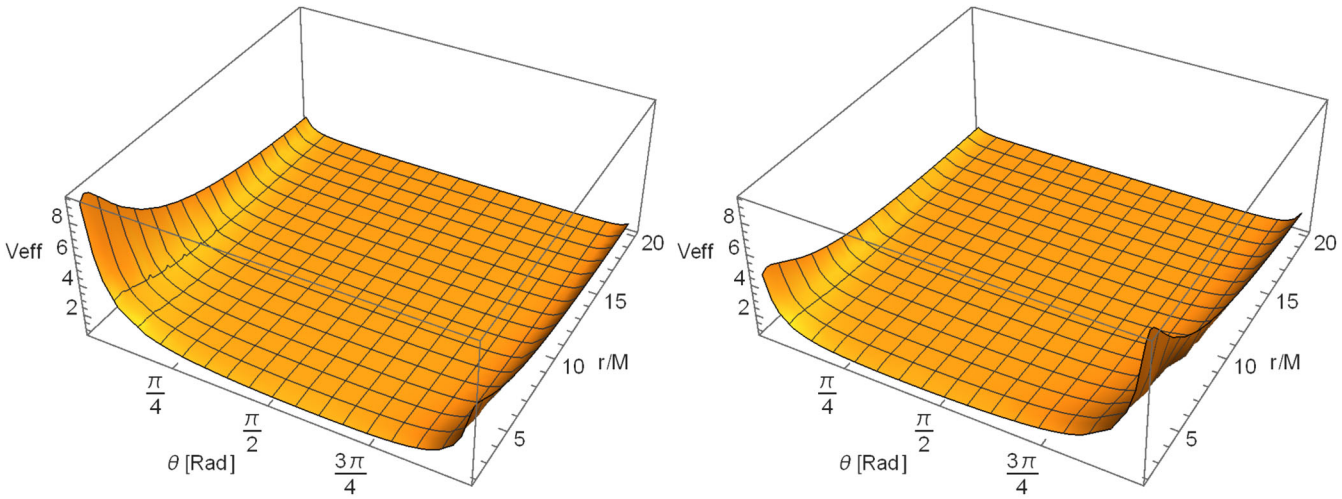

FIG. 1. Effective potential of charged particles in field of generic black hole with parameters $\alpha = 0.3$, $q = 0.5$, $\mu = 3$, $\nu = 1$ and $\mathcal{L} = 3$. On the left is parameter $e = -1$ and on the right is $e = 1$.

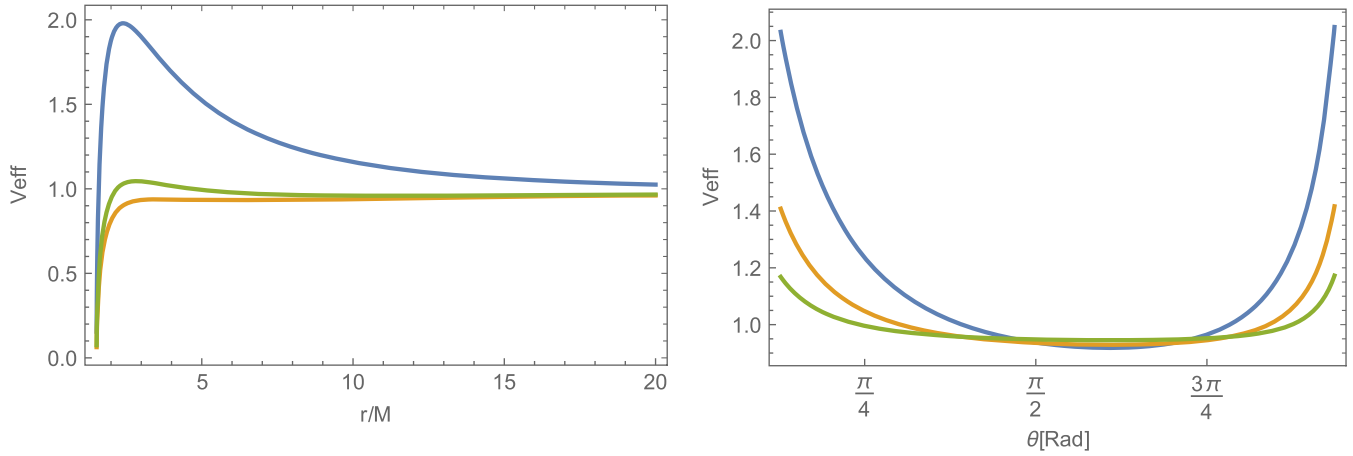

FIG. 2. The effective potential of charged particles in field of generic black hole with parameters $\alpha = 0.3$, $q = 0.5$, $\mu = 3$, $\nu = 1$, $e = -1$ and $\mathcal{L} = 3$. On the left are curves with fixed $\theta = 0.5, 1.57, 2.5$ (blue, orange, green) and on the right are curves with fixed $r = 4, 8, 13$ (blue, orange, green).

study, namely the nonexistence of the circular equatorial motion. However, we immediately see from the figures that there exist off-equatorial circular orbits that are stable against the perturbations in the radial direction, however, they could be both stable or unstable relative to the perturbation in the radial direction.

The radius of the circular orbit $r_{\rm co}$ at a fixed latitude θ is given by the solution of the relations $\mathrm{d}V_{\rm eff}(r,\theta)/\mathrm{d}r = 0$ that can be expressed in the form

$$[q^3(2-2r^\mu(q^\nu+r^\nu)^{-\frac{\mu}{\nu}})+\alpha(r-2)](\mathcal{L}-e\cos(\theta))^2 + (q^\nu+r^\nu)^{-\frac{\mu+\nu}{\nu}}[(e\cot(\theta)-\mathcal{L}\csc(\theta))^2+r^2] \times (q^3-\alpha)(q^\nu+r^\nu)^{\frac{\mu+\nu}{\nu}} - q^3 r^\mu[r^\nu-(\mu-1)q^\nu] = 0. \tag{17}$$

In the following we concentrate our attention to the case of the simplest Maxwellian NED black holes (with $\nu = 1$ and $\mu = 3$) that give the correct form of the NED in the limit of weak electromagnetic field, as only these versions could overcome the test of proper modeling the optical phenomena related to the Keplerian accretion disks [67].

B. Stable circular orbits

An innermost stable circular orbit (ISCO) with its specific angular momentum $\mathcal{L}_{\rm ISCO}$ comes from the simultaneous solution of the equations $\mathrm{d}V_{\rm eff}(r,\theta)/\mathrm{d}r = 0$ and $\mathrm{d}^2V_{\rm eff}(r,\theta)/\mathrm{d}r^2 = 0$. The ISCO position in the Schwarzschild spacetime is at $r_{\rm ISCO} = 6M$, in the generic magnetically charged black hole spacetimes, the ISCO position of uncharged particles depends on all metric parameters and it is possible to have stable circular orbits at radius lower than $r = 6M$ [69]. For example, in the generic black hole spacetime with parameters $\alpha = 0.3$, $q = 0.5$, $\mu = 3$, $\nu = 1$ the ISCO is located at $r_{\rm ISCO} = 4.46M$.

In the present paper where we study motion of electrically charged particles, also the e parameter representing

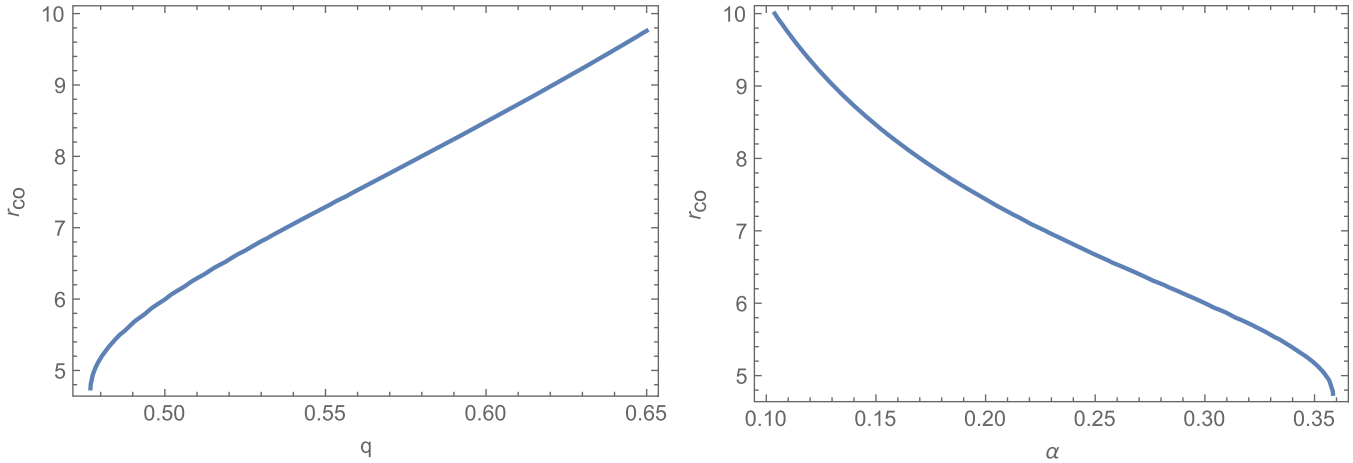

FIG. 3. The behavior of stable circular orbits $r_{\rm co}$ with parameters $\mu = 3$, $\nu = 1$, $\theta = \pi/2$, $e = 1$ and $\mathcal{L} = 3$ with respect to the parameter q with $\alpha = 0.3$ on the left panel and with respect to the parameter α with $q = 0.5$ on the right panel.

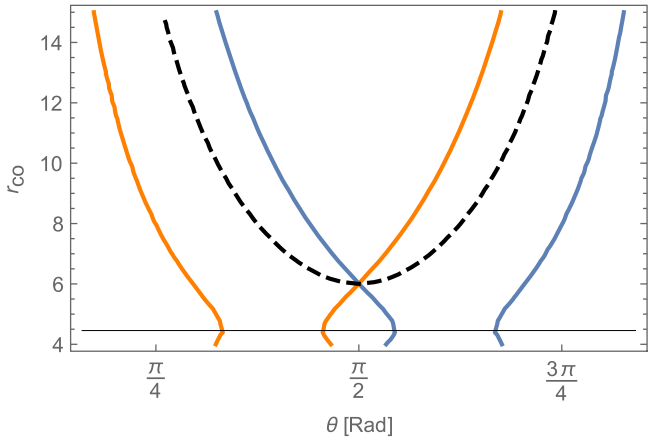

FIG. 4. The behavior of stable circular orbits r_{co} with respect to θ with parameters $\alpha = 0.3$, $q = 0.5$, $\mu = 3$, $\nu = 1$ and $\mathcal{L} = 3$. The blue curve is for parameter $e = -1$ and *orange* is for $e = 1$. A black dashed curve indicates this dependency for a neutral particle and a thin black line indicates the ISCO.

the relative intensity of the electromagnetic interaction as compared to the gravitational interaction enters the play. The effect of the α and q parameters on the stable circular orbit is examined in Fig. 3—we can see the repulsive effects of the q parameter and the attractive effects of the α parameter on the stable circular orbit.

The ISCO represents a limit on the existence of stable circular orbits and their position r_{co}. It can be seen from Fig. 4 that the stable circular orbits do not exist (for specific $\mathcal{L}$) for all values of the latitudinal coordinate θ—this statement holds for both options of the e parameter (plus and minus). Figure 5 illustrates increasing of radius of the stable circular orbit with increasing value of the specific angular momentum for both positive and negative values of the parameter e.

In Fig. 6 we present an example of stable circular orbit from three perspectives: the first and the second panel show

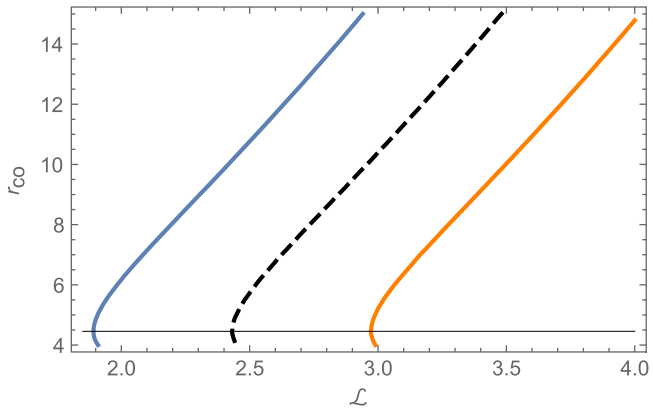

FIG. 5. The behavior of stable circular orbits r_{co} with respect to $\mathcal{L}$ with parameters $\alpha = 0.3$, $q = 0.5$, $\mu = 3$, $\nu = 1$ and $\theta = \pi/3$. The blue curve is for parameter $e = -1$ and orange is for $e = 1$. A black dashed curve indicates this dependency for a neutral particle and a thin black line indicates the ISCO.

the motion in the Cartesian coordinates in the X-Y and X-Z planes, the third panel ignores the rotational motion of the particle and represents only the motion in the radial and latitudinal directions converted to the Cartesian X-Z plane. We will continue to use this motion representation concept in the present paper. It can be immediately seen from Figure 6 that such an orbit is circular, but even if it is launched from the equatorial plane, it is not constrained by this plane, but its trajectory is tilted circle. This is caused by the presence of a magnetic field and can be observed, for example, when the charged particle moves around a Schwarzschild black hole immersed in an external magnetic monopole field.

The effective potential of the charged particle depends also on latitudinal coordinate θ. Stationary points in latitudinal direction are found by solution $\mathrm{d}V_{\mathrm{eff}}(r,\theta)/\mathrm{d}\theta = 0$. Considering the Maxwellian generic black holes with $\mu = 3$ and $\nu = 1$ and assuming the region above the black hole event horizon, we arrive at the relation

$$-2(\mathcal{L}^2 + e^2)\cos(\theta) + e\mathcal{L}[\cos(2\theta) + 3] = 0. \quad (18)$$

The extremum (minimum) of the effective potential at θ_{stat} is independent of the radial coordinate (this is also indicated at right panel of Fig. 2) and it is also independent of the parameters α and q, being dependent only on the specific angular momentum (and parameter e). The analytic solution can be written as

$$\theta_{\mathrm{stat}} = \begin{cases} \arctan\left(\frac{\sqrt{e^2-\mathcal{L}^2}}{e}\right), & \text{if } \mathcal{L} < |e|. \\ \arctan\left(\frac{\sqrt{\mathcal{L}^2-e^2}}{\mathcal{L}}\right), & \text{if } \mathcal{L} > |e|. \end{cases} \quad (19)$$

Since the arctan function acquires $\pi/2$ only at infinity, it is clear that the stationary solutions corresponding to the circular orbits cannot be found in the equatorial plane.

From the numerical analysis, it was found that the ISCO position does not depend on θ coordinate, but only the $\mathcal{L}_{\mathrm{ISCO}}$ value changes with θ. This dependence is denoted by dashed line in Fig. 7.

If we are interested in stable circular orbits, ISCO determines the lowest specific angular momentum $\mathcal{L}_{\mathrm{ISCO}}$. Thus, new limitations on $\mathcal{L}$ values appear. If the specific angular momentum at the θ_{stat} is less than $\mathcal{L}_{\mathrm{ISCO}}$ the stable circular orbit does not exist at this θ. This restriction with the dependence of $\theta_{\mathrm{stat}}(\mathcal{L})$ is presented at Fig. 7. Any value of $\mathcal{L}$ in shaded region does not satisfy condition for stable circular orbit. Values of θ_{stat} where the stable circular orbit is possible are denoted at Fig. 7 in between two black solid parallel lines.

The main result coming from Fig. 7 is that there exists circular orbits parallel to the equatorial plane ($\dot{\theta} = 0$) outside the equatorial plane. Moreover, around the generic magnetically charged black holes the electrically charged

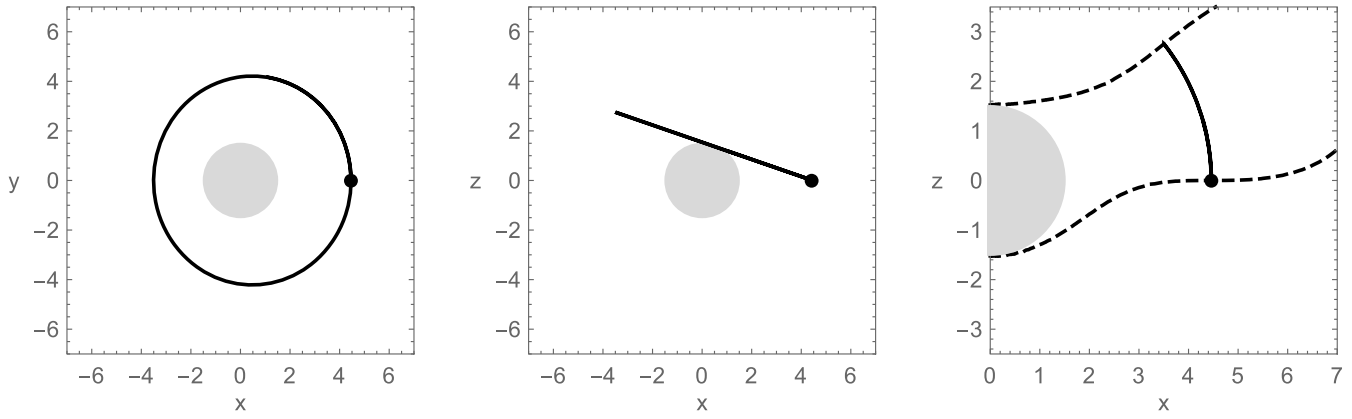

FIG. 6. The trajectories (solid curves) and movement restrictions (dashed curves) from different perspective with parameters $\alpha = 0.3$, $q = 0.5$, $\mu = 3$, $\nu = 1$, $e = 1$ and with initial conditions $\mathcal{L} = \mathcal{L}_{\mathrm{ISCO}} \doteq 2.9$, $\mathcal{E} \doteq 0.9$, $r_0 = r_{\mathrm{ISCO}} = 4.5$, $\theta_0 = \pi/2$. The left panel shows the movement in the X-Y plane, the middle panel shows the movement in the X-Z plane, and the right panel neglects the movement in the ϕ direction and shows again the movement in the X-Z plane.

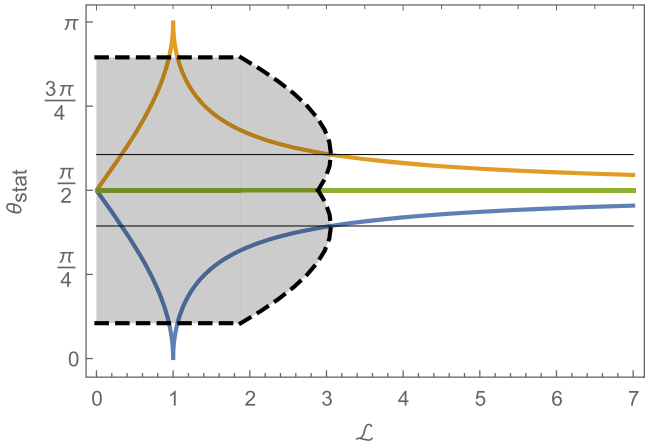

FIG. 7. The behavior of θ_{stat} with respect to $\mathcal{L}$ with parameters $\alpha = 0.3$, $q = 0.5$, $\mu = 3$, $\nu = 1$. The blue curve is for parameter $e = 1$, orange is for $e = -1$ and green one just show $\pi/2$. The black dashed line shows $\mathcal{L}_{\mathrm{ISCO}}$ at given θ. The black thin parallel solid lines indicates span of θ with possible stable circular orbit.

particle motion is not allowed in the equatorial plane, i.e., with constant $\theta = \pi/2$.

The situation near the poles is different. The reason why limiting function on $\mathcal{L}$ due to ISCO value is cut off near the poles relates to the fact that the effective potential has only a maximum for all $\mathcal{L}$—the standard concept of ISCO is missing, only unstable orbits can exist. This is evident from Fig. 8 where for the given e and various $\mathcal{L}$ the effective potentials are drawn for almost pole regions and regions where standard ISCOs can be found. Notice the existence of maxima of the effective potential at the almost pole region, and the fact that the height of the effective potential maximum is not monotonically varying with increasing $\mathcal{L}$.

Finally, in Fig. 9 we present the dependence of the position of the stable circular orbit of r_{co} on the stationary θ, i.e., the positions where there are stable circular orbits parallel to the equatorial plane.

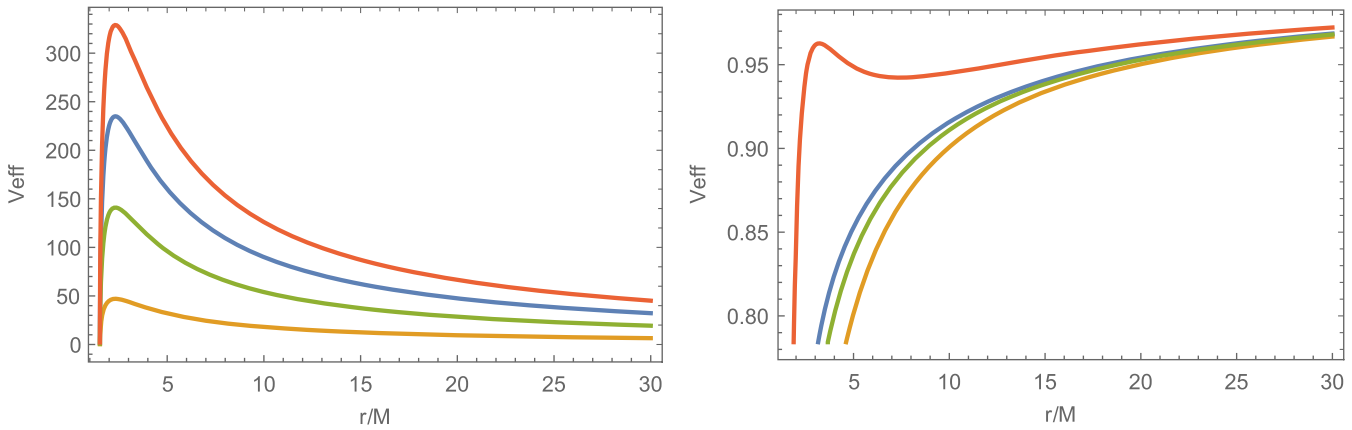

FIG. 8. The effective potential of charged particles in field of generic black hole with parameters $\alpha = 0.3$, $q = 0.5$, $\mu = 3$, $\nu = 1$, $e = 1$ and $\mathcal{L}$: $\mathcal{L} = 0$ (blue), $\mathcal{L} = 0.8$ (orange), $\mathcal{L} = 1.6$ (green) and $\mathcal{L} = 2.4$ (red). A left panel denotes $\theta = 0.001$ and a right panel denotes $\theta = 0.5$.

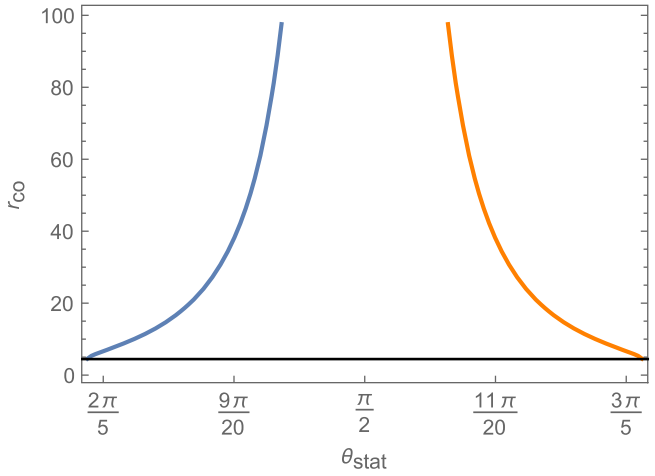

FIG. 9. The position of stable circular orbits r_{co} at stationary θ for $\alpha = 0.3$, $q = 0.5$, $\mu = 3$, $\nu = 1$ and appropriate $\mathcal{L}$ coming from (19). A blue curve is for $e = 1$ and an orange curve for $e = -1$. A black line denotes ISCO position.

C. Influence of the metric parameters on the charged particle orbits

We shortly demonstrate behavior of the epicyclic motion around circular orbits in dependence on the characteristic spacetime parameter ν governing type of the spacetime. At Fig. 10 typical trajectories in the generic black hole spacetimes for a few metric parameters fixed are presented. These are compared with the related trajectories around a Schwarzschild black hole immersed into the magnetic monopole field. It is obvious that for motion in the backgrounds with increasing parameter ν the related charged particle orbits become closer and closer to the orbits around the Schwarzschild black hole immersed into the magnetic monopole field. We can conclude that the most profound differences in the charged particle motion in comparison to the Schwarzschild case are related to the Maxwellian NED magnetically charged black holes ($\nu = 1$). These differences are suppressed for the case of the Bardeen black holes ($\nu = 2$), and almost fully suppressed in the case of Hayward black holes ($\nu = 3$).

IV. EPICYCLIC MOTION AND ITS FREQUENCIES

As mentioned in the previous chapter, we can find charged particles following the off-equatorial circular motion parallel to the equatorial plane. If such a particle is displaced from its equilibrium position at a stable circular orbit, corresponding to the minimum of the effective potential, it starts epicyclic motion around its equilibrium position. For small perturbations, the displacement coordinates $r = r_{co} + \delta r$ and $\theta = \theta_{\rm stat} + \delta\theta$ are governed by equations for linear harmonic oscillations in both the radial and latitudinal directions

$$\ddot{\delta r} + \omega_r^2 \delta r = 0, \qquad \ddot{\delta\theta} + \omega_\theta^2 \delta\theta = 0, \tag{20}$$

where the dot denotes derivative with respect to the proper time of the particle τ and ω_r and ω_θ denote the frequencies of the epicyclic oscillation as measured by a local observer. The third frequency, ω_ϕ, corresponds to the frequency of the orbital motion and is obtained from (10). Using the motion constant related to the circular orbit, the spacetime metric parameters and the gravomagnetic parameter e, we can express the epicyclic and orbital frequencies in the form

$$\omega_r^2 = \frac{1}{g_{rr}}\frac{\partial^2 H_{\rm pot}}{\partial r^2}, \qquad \omega_\theta^2 = \frac{1}{g_{\theta\theta}}\frac{\partial^2 H_{\rm pot}}{\partial \theta^2},$$
$$\omega_\phi = \frac{1}{g_{\theta\theta}}(\mathcal{L} - \bar{q}_p A_\phi). \tag{21}$$

We consider epicyclic frequencies around stationary orbits, i.e., at r_{co} and $\theta_{\rm stat}$. Using (1), (2), (8), (10)–(13) and $\mathcal{L}$ as a solution (18) in (21) with parameters $\mu = 3$ and $\nu = 1$ we get

$$\omega_r^2 = \frac{1}{2}\left\{1 - \frac{2}{r_{co}}\left[\frac{q^3}{\alpha}\left(\frac{r_{co}^3}{(q+r_{co})^3} - 1\right) + 1\right]\right\}\left[\frac{4\alpha\mathcal{E}^2}{(2q^4(q^2+3qr_{co}+3r_{co}^2)+\alpha(r_{co}-2)(q+r_{co})^3)^3}\right.$$
$$\times(-6q^8 r_{co}^2(q+r_{co})(2q^3+6q^2 r_{co}+6qr_{co}^2+3r_{co}^3)+\alpha q^4(q+r_{co})^4(q^4+5q^3 r_{co}+9qr_{co}^3+2(5q+6)qr_{co}^2+9r_{co}^4)$$
$$\left.-\alpha^2(q+r_{co})^9)+\frac{6e^2\tan^2(\theta_{\rm stat})}{r_{co}^4}\right],$$
$$\omega_\theta = \frac{e}{\cos(\theta_{\rm stat})r_{co}^2}, \qquad \omega_\phi = \frac{e}{\cos(\theta_{\rm stat})r_{co}^2}. \tag{22}$$

Notice that in this case the latitudinal epicyclic frequency coincides with the orbital frequency, as in the standard spherically symmetric Schwarzschild spacetime.

From the observational point of view, more relevant frequencies are those measured by static distant observers, denoted as f_r, f_θ and f_ϕ. The transformation between the frequencies f_a and the angular frequencies ω_a, where $a = \{r, \theta, \phi\}$ is (in the physical units)

$$f_a = \frac{1}{2\pi}\frac{c^3}{GM}\frac{\omega_a}{-g^{tt}\mathcal{E}}. \tag{23}$$

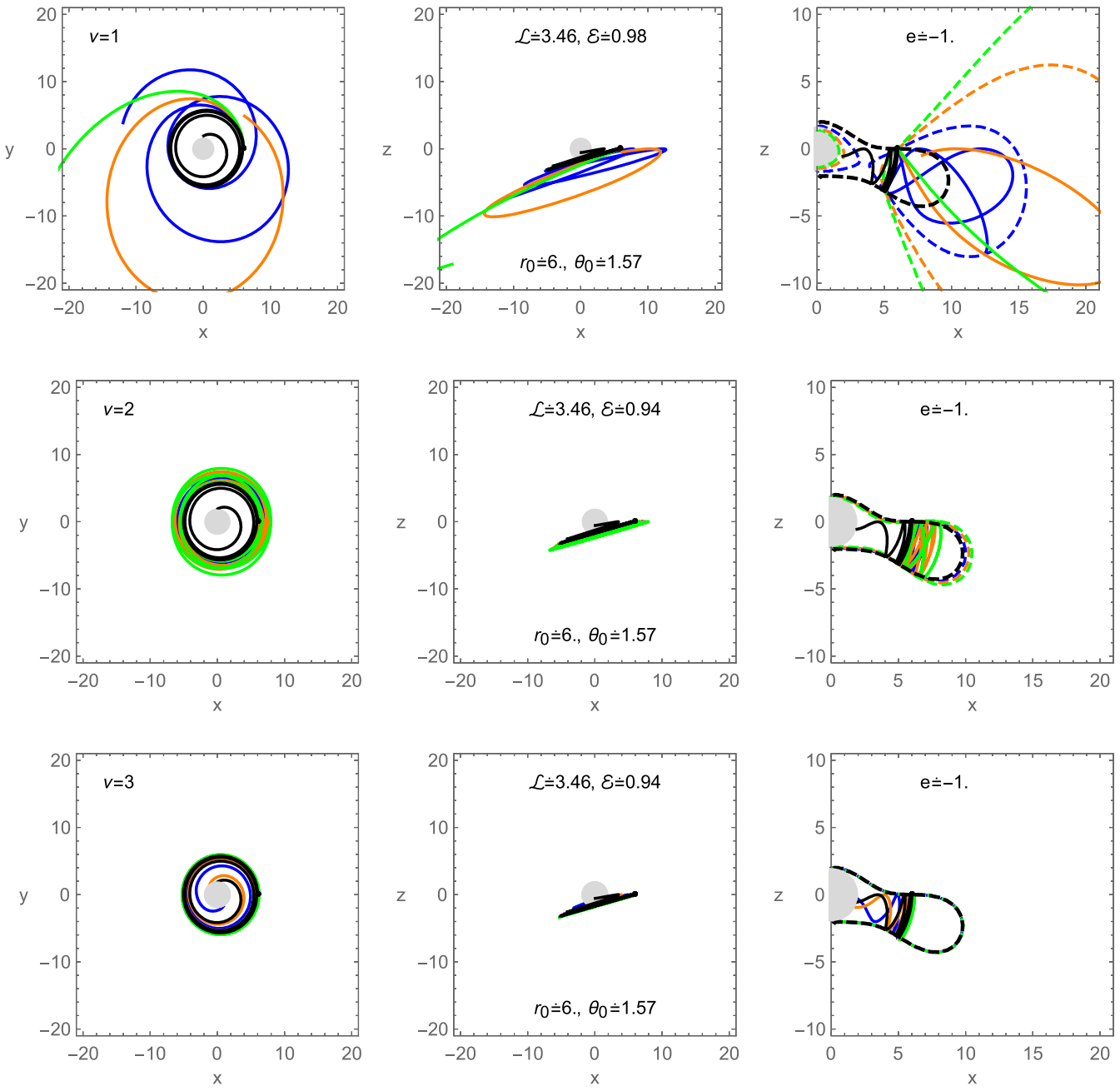

FIG. 10. The trajectories (solid curve) and movement restrictions (dashed curve) with parameters $\alpha = 0.3$, $q = 0.5$, $\nu = 1$, $e = -1$ and values μ: $\mu = 2$ (blue), $\mu = 4$ (orange), $\mu = 6$ (green) and ν: $\nu = 1, 2, 3$. The black curve describes the motion of a charged particle in Schwarzschild geometry immersed into the magnetic monopole field.

The epicyclic frequencies are the same for both the positive and negative values of parameter e and are therefore only given for $e = 1$ in left panel of Fig. 11, where they are compared to epicyclic frequencies for the Schwarzschild black hole immersed into the magnetic monopole field. The epicyclic frequencies f_θ and f_ϕ in the magnetically charged spacetimes are again identical (the blue and red dashed lines overlap), as they are in the Schwarzschild case (black dashed), but not equal to the Schwarzschild ones. The difference between the epicyclic frequencies in generic black hole case and the case of a Schwarzschild black hole immersed into the monopole magnetic field decreases with the distance from the black hole and vanishes at the $r \to \infty$ limit. Large differences arise (especially for the radial epicyclic frequency f_r) at radii close to the Schwarzschild ISCO at $r = 6M$. Another difference corresponds to the shift of the ISCO location in the generic black hole spacetime under consideration to $r = 4.46M$ and the curves in the generic case prolonged to this radius. On the right panel of Fig. 11 the ratios of the epicyclic frequencies

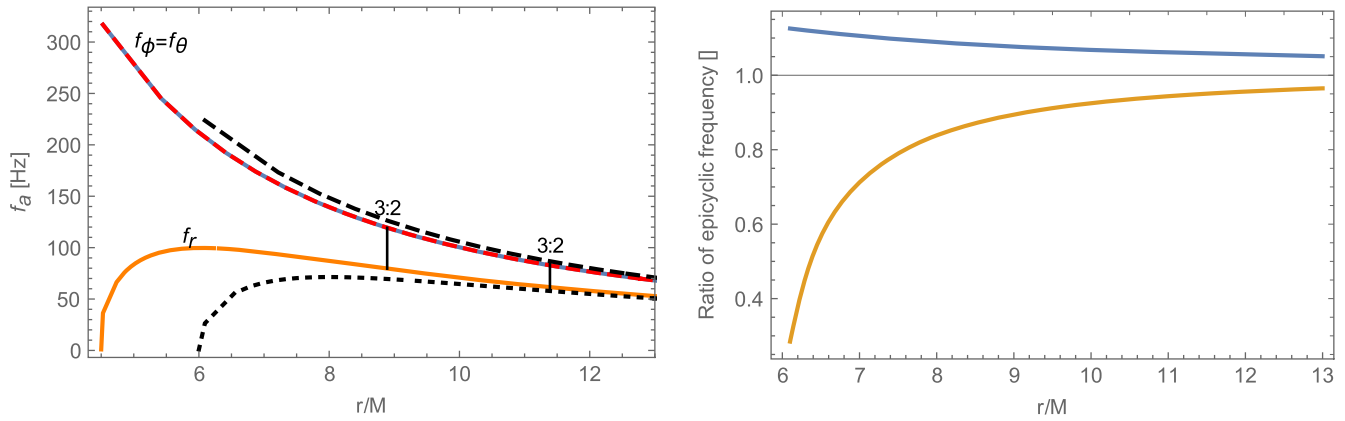

FIG. 11. On the left panel, the epicyclic frequencies in generic spacetime with parameters $\alpha = 0.3$, $q = 0.5$, $\mu = 3$, $\nu = 1$ and $e = 1$ and mass of central object $M = 10\ M_\odot$. The *blue* curve describes f_ϕ frequency, (red-dashed) curve describes f_θ frequency (both curves coincide) and orange curve describes f_r frequency. The black dashed line plots the epicyclic frequencies f_θ and f_ϕ (which are identical) and the black dotted line plots the frequency f_r in a Schwarzschild spacetime immersed into the magnetic monopole field. On the right panel is a ratio of epicyclic frequencies in Schwarzschild's spacetime and in generic spacetime. The blue curve is ratio of f_θ (and also f_ϕ) and the orange curve is ratio of f_r.

in the Schwarzschild and the generic black hole spacetimes are presented.

V. CHARGED PARTICLE OSCILLATIONS AT RESONANCE FREQUENCY RATIO 3:2 AND THE MASS-LIMIT OF MICROQUASARS

Great hopes of understanding the phenomena at strong gravity regime are placed in the observation of HF QPOs detected in many low-mass x-ray binaries (LMXB) formed by a black hole or a neutron star. In these LMXB systems, HF QPOs are sometimes observed in pairs of upper and lower frequencies (f_U, f_L) of twin peaks in the Fourier power spectra. It is interesting that in the so-called micro-quasars, LMXB containing black hole, the twin HF QPOs occurs at fixed frequencies, often in the ratio 3:2 [110].

It was found in [70] that the high-frequency peaks are very similar to the orbital frequencies of the marginally stable orbit that determines the inner edge of the Keplerian disk orbiting the central object. Consequently, it can be assumed that HF QPOs arise in areas of strong gravity.

The observation of twin HF QPO frequencies for GRO 1655-40, XTE 1550-564 and GRS 1915 + 105 gives the above-mentioned upper and lower frequency ratio

$$f_U : f_L = 3:2. \tag{24}$$

One can identify directly the frequencies f_U, f_L with the frequencies f_θ, f_r. This identification corresponds to the most relevant case of the epicyclic resonance model [71,72].

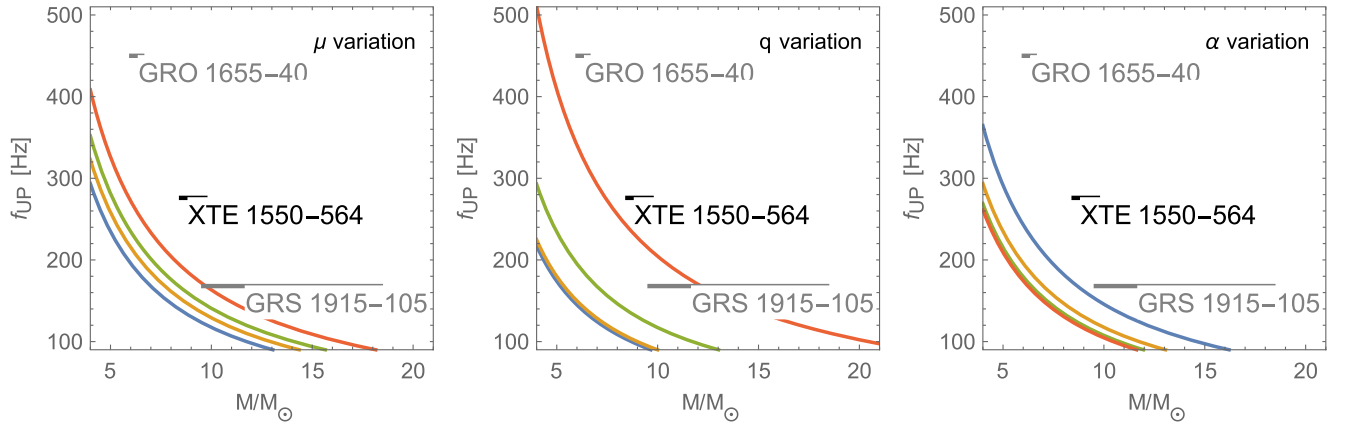

FIG. 12. The upper frequency-mass relations in generic spacetime with parameters $\alpha = 0.3$, $q = 0.5$, $\mu = 3$, $\nu = 1$ and $e = 1$. On the left panel the parameter μ is varied: $\mu = 3$ (blue), $\mu = 4$ (orange), $\mu = 5$ (green) and $\mu = 6$ (red). On the middle panel the parameter q is varied: $q = 0.3$ (blue), $q = 0.4$ (orange), $q = 0.5$ (green) and $q = 0.6$ (red). On the right panel the parameter α is varied: $\alpha = 0.2$ (blue), $\alpha = 0.3$ (orange), $\alpha = 0.4$ (green) and $\alpha = 0.5$ (red).

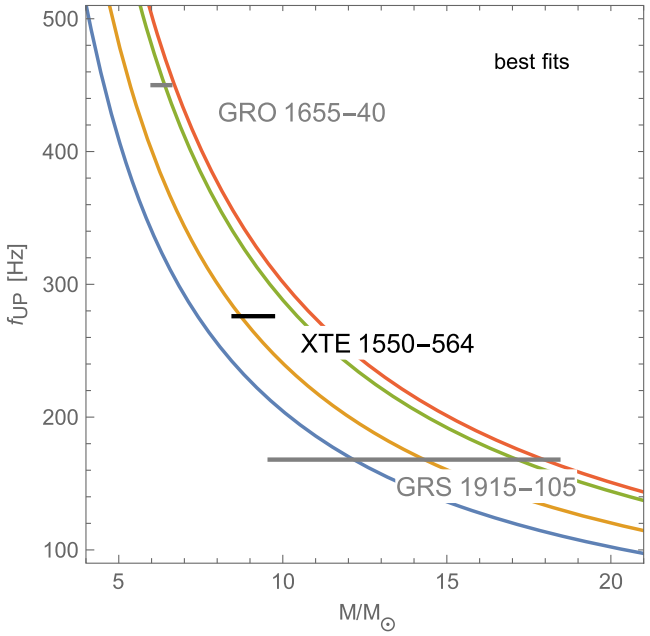

FIG. 13. The best fits of upper frequency-mass relations in generic spacetime with parameters $\nu = 1$ and $e = 1$. The blue curve is for parameters $\alpha = 0.3$, $q = 0.6$ and $\mu = 3$, the orange curve is for parameters $\alpha = 0.2$, $q = 0.5$ and $\mu = 5$, the green curve is for parameters $\alpha = 0.2$, $q = 0.5$ and $\mu = 6$ and the red curve is for parameters $\alpha = 0.3$, $q = 0.6$ and $\mu = 4$.

Now we plan to show the influence of the μ, q and α parameters on the relation of the upper HF QPO frequency and mass of the central object with respect to real astronomical observational data. The μ and q parameters appear to increase the upper frequency relative to the mass of the central object, while the α parameter decreases this frequency as shown in Fig. 12. The q parameter has the strongest impact, however, it is important to note that one cannot increase the q parameter indefinitely if one wants to deal with the black hole (an object having at least one horizon). There is no analytical expression for the marginal q, but numerical results for several metric parameter variations can be found in [69]. The best fits of parameter μ, q and α of upper frequency-mass relations on the observation data for GRO 1655-40, XTE 1550-564 and GRS $1915+105$ are presented in Fig. 13.

VI. MAGNETIZED PARTICLE MOTION AROUND MAGNETICALLY CHARGED BLACK HOLES IN GR COUPLED TO NED

In this section, we plan to study the dynamics of magnetized particles around the generic magnetically charged black holes.

Using potential (4) one may immediately obtain the nonzero component of the electromagnetic field tensor by the relation $F_{\mu\nu} = A_{\nu,\mu} - A_{\mu,\nu}$ in the standard form

$$F_{\theta\phi} = -Q_m \sin\theta. \tag{25}$$

We calculate the orthonormal components of the magnetic field measured by zero angular momentum observer (ZAMO) in the black hole spacetime (1) using the relation

$$B^\alpha = \frac{1}{2}\eta^{\alpha\beta\sigma\mu}F_{\beta\sigma}w_\mu, \tag{26}$$

where w_μ is velocity of the observer who measure the magnetic field, $\eta_{\alpha\beta\sigma\gamma}$ is the pseudotensorial form of the Levi-Civita symbol $\epsilon_{\alpha\beta\sigma\gamma}$ with the relations

$$\eta_{\alpha\beta\sigma\gamma} = \sqrt{-g}\epsilon_{\alpha\beta\sigma\gamma} \qquad \eta^{\alpha\beta\sigma\gamma} = -\frac{1}{\sqrt{-g}}\epsilon^{\alpha\beta\sigma\gamma}, \tag{27}$$

and $g = \det|g_{\mu\nu}| = -r^4\sin^2\theta$ for spacetime metric (1) and

$$\epsilon_{\alpha\beta\sigma\gamma} = \begin{cases} +1, & \text{for even permutations} \\ -1, & \text{for odd permutations} \\ 0, & \text{for the other combinations} \end{cases}, \tag{28}$$

than

$$B^{\hat{r}} = \frac{Q_m}{r^2}. \tag{29}$$

Equation (29) implies that the radial component of the magnetic field around magnetically charged black holes is not affected by the spacetime curvature and looks like the standard Newtonian expression.

One way to test spacetime around compact objects is though study of test particle motion. In order to explore properties of magnetically charged black holes, we aimed to describe the motion of magnetized particles around the generic black hole using the following Hamilton Jacobi equation [100]:

$$g^{\mu\nu}\frac{\partial\mathcal{S}}{\partial x^\mu}\frac{\partial\mathcal{S}}{\partial x^\nu} = -(m - \frac{1}{2}\mathcal{D}^{\mu\nu}F_{\mu\nu})^2, \tag{30}$$

with the term $\mathcal{D}^{\mu\nu}\mathcal{F}_{\mu\nu}$ which characterizes the interaction between the magnetized particle and the magnetic field generated by the NED field. Assuming the structure of the magnetized particle's magnetic moment/field is dipolar, the polarization tensor $\mathcal{D}^{\alpha\beta}$ subjects to the following condition:

$$\mathcal{D}^{\alpha\beta} = \eta^{\alpha\beta\sigma\nu}u_\sigma\mu_\nu, \qquad \mathcal{D}^{\alpha\beta}u_\beta = 0, \tag{31}$$

where μ^ν and u_μ is the four-vector of dipole moment and velocity of the magnetized particle. It is possible to determine the interaction term of the Hamilton-Jacobi equation (30) using the standard relation between the electromagnetic field tensor $F_{\alpha\beta}$ and components of electric E_α and magnetic B^α fields

$$F_{\alpha\beta} = w_\alpha E_\beta - w_\beta E_\alpha - \eta_{\alpha\beta\sigma\gamma} w^\sigma B^\gamma. \tag{32}$$

Taking into account the condition given in (31) and nonzero components of the electromagnetic field tensor we have

$$\mathcal{D}^{\alpha\beta} F_{\alpha\beta} = 2\mu_\alpha B^\alpha = 2\mu^{\hat{\alpha}} B_{\hat{\alpha}} \tag{33}$$

where $\mu^{\hat{\alpha}}$ and $B_{\hat{\alpha}}$ are measurable values of the proper magnetic dipole moment of the magnetized particle and the magnetic field generated in the presence of NED by the observer in ZAMO framework.

In the study of the dynamics of the magnetized particle around the generic black hole, we will let the direction of the magnetic dipole moment of the magnetized particle to be parallel to the equatorial plane as well as to the magnetic field of the generic black hole. The components then are $\mu^i = (\mu^r, 0, 0)$, the other configurations of magnetic dipole moment components cannot provide the magnetized particle with a stable equilibrium. In fact, in the equilibrium of the minimum energy of the magnetic interactions the direction of magnetic field lines and magnetic dipole moment of the magnetized particle have to be the same. Moreover, the second part of the condition (31) allows us to study the particle motion in ZAMO framework and the choice of the observer velocity may help to avoid a relative motion problem. The magnitude of the constant magnetic moment is constant and is maintained during the motion. One may rewrite the interaction using (33) and (25) in the following form:

$$\mathcal{D}^{\alpha\beta} F_{\alpha\beta} = \frac{2\mu Q_m}{r^2}, \tag{34}$$

where $\mu = |\mu| = \sqrt{\mu_i \mu^{\hat{i}}}$ is the norm of the magnetic dipole moment of the magnetized particle.

Since, the axial symmetric configuration of the proper magnetic field of the generic black hole coupled the NED does not break the spacetime symmetries and, therefore, there are still two conserved quantities: energy $p_t = -E$ and angular momentum $p_\phi = l$. Then it is possible to rewrite the expression for the action of the magnetized particle so that one can separate variables in the Hamilton-Jacobi equation (30) as

$$\mathcal{S} = -Et + l\phi + \mathcal{S}_r(r). \tag{35}$$

The radial motion of a magnetized particle at the equatorial plane, where $\theta = \pi/2$, with $p_\theta = 0$, using (33), (30) and the action (35) gives the following form:

$$\dot{r}^2 = \mathcal{E}^2 - V_{\rm eff}(r; \mathcal{L}, \mathcal{B}). \tag{36}$$

The effective potential has the form

$$V_{\rm eff}(r; \mathcal{L}, \mathcal{B}, q) = f(r)\left[\left(1 - \frac{\mathcal{B}}{r^2}\right)^2 + \frac{\mathcal{L}^2}{r^2}\right] \tag{37}$$

where the relation

$$\mathcal{B} = \frac{\mu}{mM} Q_m = \beta \frac{q^2}{\sqrt{2\alpha}}$$

is a magnetic interaction parameter which is responsible for the interaction between magnetized particles and the proper magnetic field of the generic black hole and $\beta = \mu/(mM)$ is dimensionless parameter that characterizes the magnetized particle and the central black hole parameters are always positive for the system when magnetized neutron star is treated as test magnetized particle orbiting around a supermassive black hole

$$\beta = \frac{B_{\rm NS} R_{\rm NS}^3}{2 m_{\rm NS} M_{\rm SMBH}} \simeq 0.18 \left(\frac{B_{\rm NS}}{10^{12}\ {\rm G}}\right) \left(\frac{R_{\rm NS}}{10^6\ {\rm cm}}\right) \left(\frac{m_{\rm NS}}{M_\odot}\right)^{-1} \left(\frac{M_{\rm SMBH}}{10^6\ M_\odot}\right)^{-1}. \tag{38}$$

The circular stable orbits of the magnetized particle around the central object can be defined by the standard conditions as

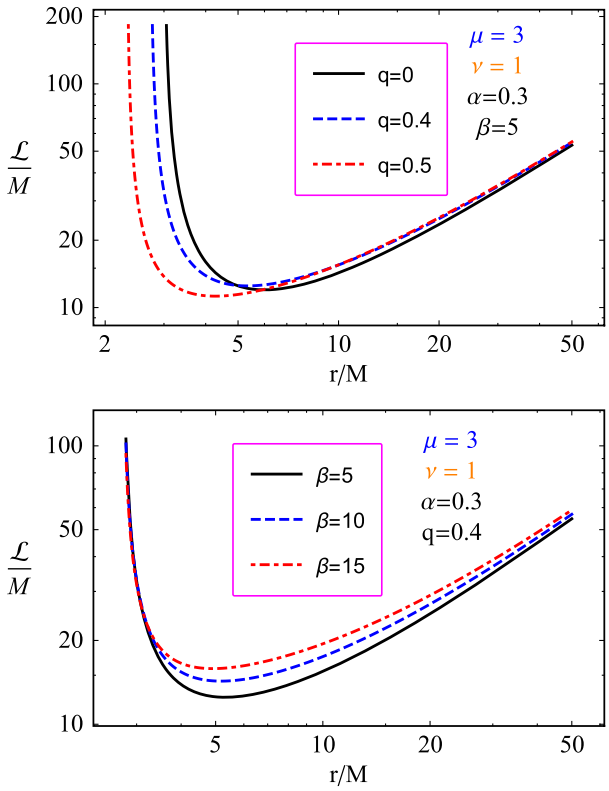

FIG. 14. The radial dependence of the specific angular momentum for circular orbits for the different values of magnetic charge parameter and the parameter β.

$$V'_{\rm eff} = 0, \qquad V''_{\rm eff} \geq 0. \tag{39}$$

Specific angular momentum and energy of the magnetized particle along the circular orbits can be expressed by the following expressions:

$$\mathcal{L}^2 = -\frac{(r^2-\mathcal{B})(r(r^2-\mathcal{B})f'(r)+4\mathcal{B}f(r))}{r^2(rf'(r)-2f(r))} \tag{40}$$

$$\mathcal{E}^2 = \frac{2f(r)^2(\mathcal{B}^2-r^4)}{r^4(rf'(r)-2f(r))}. \tag{41}$$

Figure 14 shows the radial dependence of the specific angular momentum of a magnetized particle around the generic black hole. One can see from this figure that the increase of the magnetic charge of the black hole (the parameter β) decreases (increases) the minimum value of the specific angular momentum of the magnetized particle. Moreover, as the increase of both magnetic charge parameter and the parameter β the distance where the specific angular momentum is minimum decreases.

The radial dependence of the specific energy of the magnetized particle for the different values of the parameter β and the magnetic charge parameter is shown in Fig. 15. One can see from Fig. 15 that with the increase of the parameters q and β ISCO radius shifts towards the central black hole and the minimum values of the specific energy decreases.

One can easily obtain equation for ISCO taking into account the conditions (39) for the effective potential (37) in the following form:

$$2r^2(\mathcal{B}^2-r^4)f'(r)^2+8\mathcal{B}^2f(r)^2+rf(r) \times [r(r^4-\mathcal{B}^2)f''(r)+(3r^4-7\mathcal{B}^2)f'(r)] \geq 0. \tag{42}$$

Since, it is hard to analytically solve Eq. (42) with respect to the radial coordinate we can only analyze the ISCO profiles presenting them in plot form.

The dependence of ISCO radius on the magnetic charge parameter for the different values of the parameters β and ν is presented in Fig. 16, where $\mu = 3$, $\alpha = 0.3$. One can see from the figures the increase of the parameter β increases the rate of decreasing of ISCO radius and the comparison of the cases $\nu = 1$ and $\nu = 2$ shows that effect of the parameter β is stronger at $\nu = 2$ than at $\nu = 1$.

Figure 17 demonstrates dependence of ISCO radius on the parameter β for the different values of magnetic charge

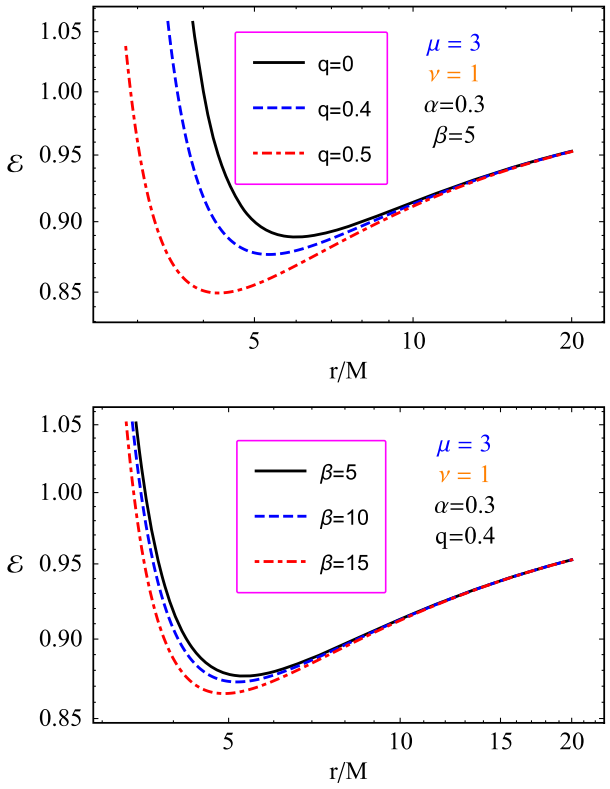

FIG. 15. The radial dependence of the specific energy for circular orbits for the different values of magnetic charge parameter and the parameter β.

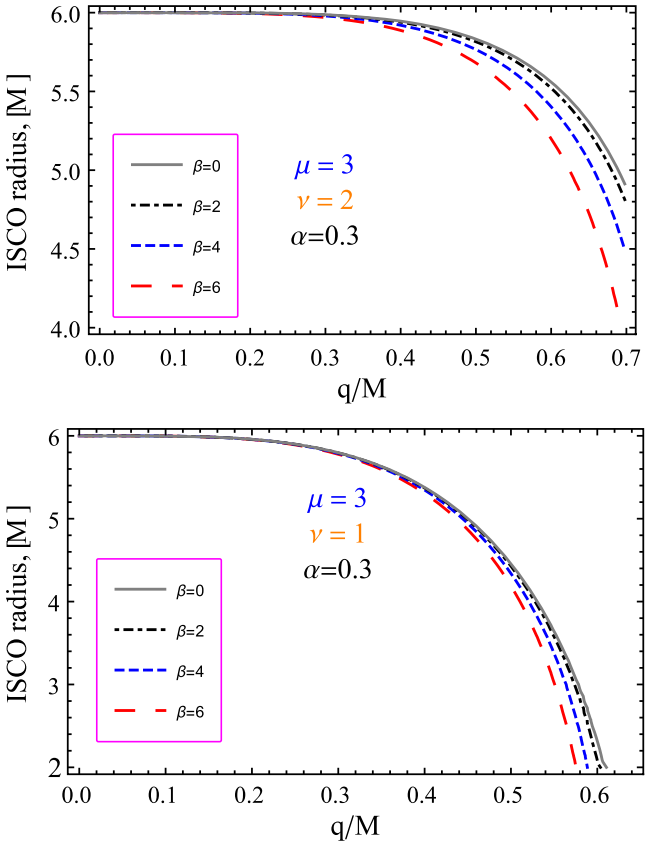

FIG. 16. ISCO radius of a magnetized particle around the generic regular black holes for the value of the parameter $\nu = 1$ and $\nu = 2$.

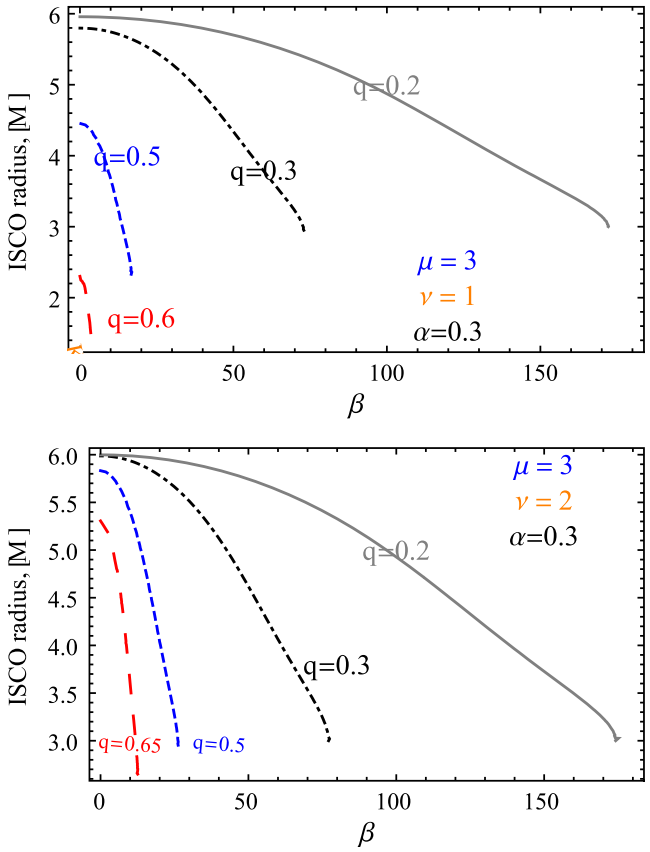

FIG. 17. ISCO radius of a magnetized particle around the generic regular black holes for the value of the parameter $\nu = 1$ and $\nu = 2$.

parameter q and the parameter ν, at the values of the parameters $\mu = 3$ and $\alpha = 0.3$. One may observe that ISCO radius decreases with increase of both the magnetic charge parameter q and the parameter β. Our numerical calculations show that at the maximum value of the magnetic charge parameter, ISCO disappears for the magnetized particle, for any values of the β parameter. Moreover there is an upper limit for the parameter β for the existence of ISCO radius at $q < q_{\max}$ and the upper limit value for the parameter β decreases with the increase of the magnetic charge parameter q. It is meant that the magnetized particle orbit become unstable due to interaction between the magnetic field and magnetic moment of the particle.

VII. ASTROPHYSICAL APPLICATIONS

Testing various theories of gravity in the strong field regime considering dynamics of test particles is always actual and can help to explore nature of gravitational and electromagnetic fields around the central black hole and to estimate the fundamental parameters of the black hole. One of the observational properties of the test particle motion is the behavior of ISCO and phenomena concerning QPOs. If we have multiple gravity models, observational data (such as ISCO positions or effects associated with QPOs) are not able to clearly distinguish which model's effects dominate. Thus, it may be the case that different characteristics of these models have a similar effect on the behaviors of test particle dynamics. The problem that the astronomical observations do not care about which model of gravity plays important role in the observations of ISCO position and frequencies of QPOs, which means two different theories of gravity can give the same values of ISCO radius or QPO frequencies and mimic each other. In order to distinguish the effects of the parameters of different theories of gravity one can compare the observational parameters of dynamics of the test particles. We aimed to study how the generic black hole effects can mimic a rotation of Kerr black hole. Analysis of solution for ISCO radius of magnetized particles around the generic black holes and test particles around Kerr black hole and the magnetized particles around Schwarzschild black hole immersed in an external magnetic field can help to find out how the generic black holes magnetic charge parameter mimics the effects of the spin of Kerr black hole.

ISCO radius of the test particles for retrograde and prograde orbits around Kerr BH can be expressed as [111]

$$r_{\rm isco} = 3 + Z_2 \pm \sqrt{(3 - Z_1)(3 + Z_1 + 2Z_2)}, \quad (43)$$

with

$$Z_1 = 1 + (\sqrt[3]{1+a} + \sqrt[3]{1-a})\sqrt[3]{1-a^2},$$
$$Z_2 = \sqrt{3a^2 + Z_1^2}.$$

We plan to perform the above-mentioned study of ISCO analyzing considering the motion of the magnetar SRG (PSR) J1745–2900 orbiting around the Sgr A* as approximated test magnetized particle with the parameters $\beta = 10$ assuming the Sgr A* black holes as (i) Kerr black hole with spin parameter a, (ii) generic black hole and (iii) Schwarzschild black hole immersed in the magnetic field one by one.

For the system of the magnetar called SRG (PSR) J1745–2900 orbiting around supermassive black hole Sgr A* with mass $M \approx 3.8 \times 10^6\ M_\odot$, discovered in 2013 in radio band [112], the value of the parameter β for the magnetar can be easily estimated based on the observational data analysis in [112] that shows the magnetic dipole moment of the magnetar $\mu \approx 1.6 \times 10^{32}$ G $\cdot$ cm^3 and mass $m \approx 1.5\ M_\odot$ as

$$\beta = \frac{\mu_{\rm PSR\,J1745-2900}}{m_{\rm PSR\,J1745-2900} M_{\rm SgrA*}} \approx 10.2. \quad (44)$$

Figure 18 presents profiles of ISCO radius of a magnetized particles around: Kerr black hole; Schwarzschild black hole immersed in the external magnetic field and the

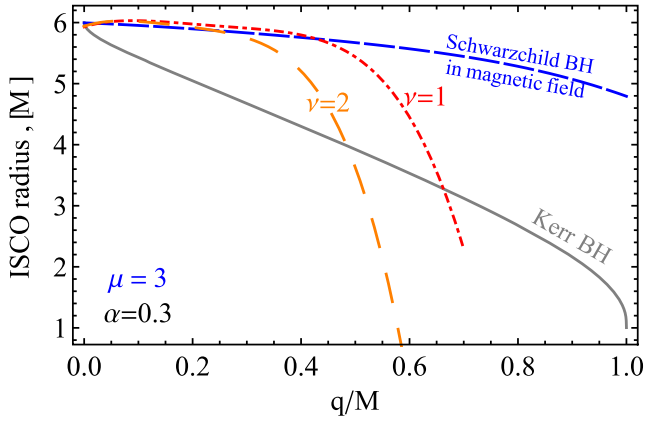

FIG. 18. ISCO radius of a magnetized particle around the generic magnetically charged regular black hole, Kerr black hole and Schwarzschild black hole immersed in the external magnetic field for the values of the parameter $\nu = 1$ and $\nu = 2$.

generic black hole at their proper parameters $a/M \in (0, 1)$, $q \in (0, q_{\max}(\nu))$ and $\beta \in (0, 1)$, respectively. One may see that ISCO radius can be the same for the different approaches, arising indistinguishable nature of the black holes.

A. Generic black hole vs Kerr black hole

In this subsection we study the motion of magnetized and nonmagnetized particles around the generic and Kerr black holes, respectively and show how the magnetic charge parameter of the black hole mimics spin of Kerr black hole and gives the same ISCO radius.

Figure 19 illustrates the relation between rotation parameter of Kerr black hole and magnetic charge parameter of the generic black hole for the same ISCO radius. One can see that when the parameter $\nu = 1$ the magnetic charge parameter can mimic the spin parameter up to $a_{\max} = 1$, for the particle with $\beta = 10$ the spin parameter $a = 0.865694$,

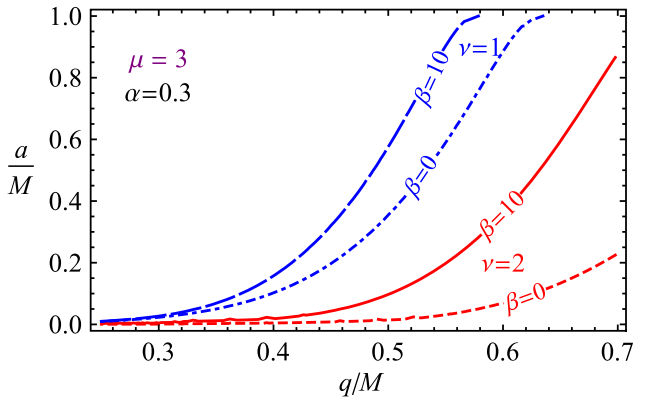

FIG. 19. Relations between spin parameter and magnetic charge parameter giving the same ISCO radius for the different values of the magnetic coupling parameter and the parameter ν at $\mu = 3$ and $\beta = 10$.

but for neutral (nonmagnetized) particles, it is up to $a = 0.224659$. When the parameter $\nu = 2$ the spin parameter can mimic the charge parameter up to $q = q_{\max} = 0.697848$ and for particles with $\beta = 10$ the magnetic charge parameter up to $q = 0.578575$, but for $\beta = 0$, it is up to $q = 0.634811$.

B. Generic black hole vs Schwarzschild black hole in magnetic field

In this subsection, we will compare the motion of magnetized particles around generic black hole and Schwarzschild black hole immersed in an external uniform magnetic field, focusing on how the magnetic charge parameter can mimic the effect of external magnetic field parameter giving the same ISCO radius for the magnetized particle. The dynamics of magnetized particles around Schwarzschild black hole in the external magnetic field have been investigated in [100] in detail. One can estimate the magnetic coupling parameter as

$$\mathfrak{B} = \frac{2\mu B_0}{m} = \frac{B_{\rm NS} R_{\rm NS}^3 B_{\rm ext}}{m_{\rm NS}}$$

for a pulsar orbiting around a supermassive black hole. This value of the interaction parameter for the magnetar SRG (PSR) J1745–29 orbiting around Sgr A* is

$$\mathfrak{B}_{\rm PSR\,J1745-2900} \simeq 0.716 \left(\frac{B_{\rm ext}}{10\ {\rm G}}\right). \tag{45}$$

In previous works [102,104] we have shown that magnetized particle orbits cannot be stable at $\mathfrak{B} \geq 1$. We will study the magnetars ISCO in field Sgr A*, for $\mathfrak{B} < 1$ ($B_{\rm ext} \lesssim 14$ G). This indicates that a magnetar with the surface magnetic field at the order of $B_{\rm surf} > 10^{14}$ G cannot be in stable orbits around the central supermassive black hole when the external magnetic field is more than the order of 10 G. Since the expected magnetic field near Sgr A* is around 100 G, the magnetic coupling parameter for the magnetar (SGR) PSR J1745-2900 is $\mathfrak{B} \simeq 7.16$ and one may predict that we observe a pulsar with the surface magnetic field less than 10^{12} G. Nonobservability of radio pulsars and magnetars on the central part of our galaxy in close vicinity of SgrA* can be caused by either their nonexistence in the region close to ISCO or scattering of radio signals broadening them and leads to pulsar's signal disappearance. The detailed analysis performed here shows that the interaction of ambient magnetic field with magnetar's (pulsar's) magnetic moment is so strong that magnetar's orbit in close vicinity of SgrA* becomes very unstable and unlikely to search magnetars there. The only opportunity is to look for the radio pulsars with low surface magnetic field in that area.

Figure 20 demonstrates relations between magnetic coupling parameter and magnetic charge parameter of

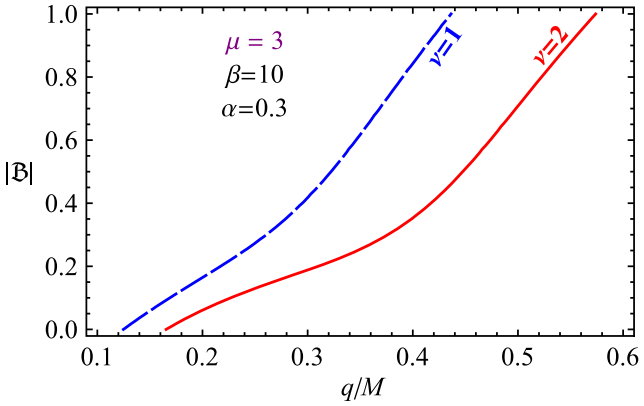

FIG. 20. Relations between magnetic coupling parameter and magnetic charge parameter giving the same ISCO radius for the different values of the magnetic coupling parameter and the parameter ν at $\mu = 3$ and $\beta = 10$.

the generic black hole and we see that for $\beta = 10$ and the parameter $\nu = 1$ and $\nu = 2$ the magnetic coupling parameter can mimic the magnetic charge parameter of the black hole in the range $q \in (0.144324, 0.4368)$ and $q \in (0.165447, 0.574278)$, respectively. This analysis allows us to distinguish the magnetized particles orbiting around Schwarzschild black hole in the presence of the external magnetic field from the magnetized particle orbiting around the magnetically charged generic black hole.

VIII. CONCLUSION

In this work we have investigated the motion of electrically charged particles in the singular generic magnetically charged black hole spacetime (1) with mass function (2), found as solution of the Einstein field equations coupled to nonlinear electrodynamics, continuing thus the work [69], where we have investigated the motion of photons and neutral particles in the same spacetime.

We introduced this spacetime and its main characteristics in Sec. II. It is also important to recall we mainly focused on generic spacetime with parameters $\mu = 3$ and $\nu = 1$, unless otherwise stated.

In Sec. III were introduced Hamiltonian, the equations governing the motion of charged particles and the effective potential and we investigated these equations and effective potential to get important information about specifications of the charged particle motion in this spacetime. The first significant feature of the effective potential is the existence of some symmetry in parameters e (15) and θ. If we change a sign in e we get the same effective potential if $\theta \to \pi - \theta$. In other words, charged particles with a positive e behave on the "north" ($\theta \in < 0, \pi/2 >$) as well as particles with a negative e on the "south" ($\theta \in < \pi/2, \pi >$) and vice versa, as one can see in Fig. 1.

We examined the stationary points of the effective potential in both variables, r (stable circular orbit) and θ (motion parallel to the equatorial plane). We found that while a stable circular orbit depends on θ (see Fig. 4), $\mathcal{L}$ (see Fig. 5) and other spacetime parameters, stationary points in the θ direction depend only on $\mathcal{L}$ (19) (see Fig. 7). It can be seen from Fig. 4 that not every θ has a stable circular orbit.

Concerning the stationary points for θ, whose $\mathcal{L}$ value is greater than the $\mathcal{L}_{\rm ISCO}$, we see the limitation shown in Fig. 7 by the gray area enclosed by a black dashed line. There do not exist stable circular orbits in this area. In Figure 7, we also see the indicated range of θ (in between two thin lines), in which there are stationary θ with the possible existence of the stable circular orbit. It is interesting [which also follows from (19)] that there is no stationary θ in the equatorial plane.

It can be seen from Fig. 9 that the position of the stable circular orbit moves away from the ISCO position as θ approaches the equatorial plane and the nearest stable circular orbits are at about $\theta = 2\pi/5$ for $e = 1$ and $\theta = 3\pi/5$ for $e = -1$.

We also investigated an influence of other spacetime parameters on r_{co} and found that the stable circular orbit is pushed out with increasing charge parameter q, on the other hand, the stable circular orbit is pushed inward with increasing parameter α, see Figure 3.

At the end of Sec. III, we compared particle trajectories for various μ and ν with trajectories in spacetime of Schwarzschild black hole immersed into the magnetic monopole field, Fig. 10. Comparing these trajectories shows that for $\nu \geq 2$, the particle trajectories are almost the same as in Schwarzschild's spacetime immersed into the magnetic monopole field and parameter μ does not have strong affect.

In Sec. IV we focused on the behavior of epicyclic frequencies. We studied how they behave and found that epicyclic frequencies do not depend on the sign of e and that the epicyclic frequencies in the θ and ϕ directions are identical. We also compared these frequencies with the results for spacetime of Schwarzschild black hole immersed into the magnetic monopole field. This is shown in Fig. 11 (the comparison is on the left panel and the ratio is on the right panel). If we ignore the fact that the ISCO in generic spacetime is closer to the center than in the Schwarzschild one and we are able to find epicyclic frequencies closer to the black hole, it is clear from the right panel of Fig. 11 that at $r = 6M$ the epicyclic frequencies in Schwarzschild's spacetime immersed into the magnetic monopole field in θ and ϕ direction are approximately 15% larger than in generic spacetime and with increasing r this gap decreases. Conversely, epicyclic frequencies in the r direction are much larger in generic spacetime around $r = 6M$. With the increasing r, these differences are eliminated.

Moreover, we have studied the dynamics of magnetized particles around the magnetically charged generic black hole at the equatorial plane. Analysis of ISCO radius of the

magnetized particle shows that the radius decreases with increase of the magnetic charge parameter and the newly introduced interaction parameter β, and the ISCO disappears at $q \geq q_{\max}(\nu)$ at some values of the upper limit for the parameter β. As an astrophysical application of the limits given by ISCO we give the mimic cases of degeneracy of the magnetic charge parameter with the magnetic interaction and the black hole spin parameters. Our study shows that the effect of parameter q can totally coincide with the effect of spin parameter a, one may distinguish the parameters when $q \geq 0.578575$ for the magnetized object with $\beta = 10$ (here we treated the magnetar PSR J1745 − 2900 as magnetized particle) at $\nu = 1$, however, for the case $\nu = 2$ the black hole spin parameter cannot mimic the magnetic charge parameter q for the same ISCO radius when $a > 0.224659$ for nonmagnetized (neutral) particles and the particle with $\beta = 10$ at $a > 0.865694$. The comparison of effects of the charge parameter and magnetic interaction parameter $\mathfrak{B}$ shows that for the magnetar with $\beta = 10$ and the parameters $\nu = 1$ and $\nu = 2$, the magnetic coupling parameter $\mathfrak{B}$ can mimic the magnetic charge parameter of the black hole in the range $q \in (0.144324, 0.4368)$ and $q \in (0.165447, 0.574278)$, respectively, in the range $0 \leq |\mathfrak{B}| \leq 1$. Finally, we analyzed the existence of radio pulsars and magnetars around SgrA* and predicted that one may observe radio pulsars with the surface magnetic field $10^8 \div 10^{12}$ G in stable orbits as recycled pulsars around SgrA* and magnetars with the surface magnetic field more that 10^{14} G cannot exist at close distances due to instability caused by magnetic interaction while magnetic field in the vicinity of SgrA* is about 100 G.

ACKNOWLEDGMENTS

We acknowledge the institutional support of Silesian University in Opava and Grant No. SGS/12/2019. This research is supported by Grants No. VA-FA-F-2-008 and No. MRB-AN-2019-29 of the Uzbekistan Ministry for Innovative Development, and by the Abdus Salam International Centre for Theoretical Physics. This research is partially supported by an Erasmus + exchange grant between SU and NUUz. One of the authors (J. V.) was supported by the Czech Grant No. LTC18058. A. A. is supported by PIFI fund of Chinese Academy of Sciences.

[1] S. Hawking and G. Ellis, *The Large Scale Structure of Space-Time*, Cambridge Monographs on Mathematical Physics (Cambridge University Press, Cambridge, England, 1975).
[2] F. de Felice, Astron. Astrophys. **34**, 15 (1974).
[3] Z. Stuchlik, Bull. Astron. Inst. Czech. **31**, 129 (1980).
[4] J. Bicak, Z. Stuchlik, and V. Balek, Bull. Astron. Inst. Czech. **40**, 65 (1989).
[5] P. Horava, in *The Davis Meeting On Cosmic Inflation* (2003), p. 23.
[6] E. G. Gimon and P. Hořava, Phys. Lett. B **672**, 299 (2009).
[7] Z. Stuchlík, S. Hledík, and K. Truparová, Classical Quantum Gravity **28**, 155017 (2011).
[8] Z. Stuchlík and J. Schee, Classical Quantum Gravity **30**, 075012 (2013).
[9] M. Blaschke and Z. Stuchlík, Phys. Rev. D **94**, 086006 (2016).
[10] Z. Stuchlík, M. Blaschke, and J. Schee, Phys. Rev. D **96**, 104050 (2017).
[11] D. Pugliese, H. Quevedo, and R. Ruffini, Phys. Rev. D **83**, 104052 (2011).
[12] G. W. Gibbons and S. W. Hawking, Phys. Rev. D **15**, 2738 (1977).
[13] Z. Stuchlik, Bull. Astron. Inst. Czech. **34**, 129 (1983).
[14] Z. Stuchlík and S. Hledík, Phys. Rev. D **60**, 044006 (1999).
[15] Z. Stuchlík and S. Hledik, Acta Phys. Slovaca **52**, 363 (2002).
[16] Z. Stuchlík, J. Schee, B. Toshmatov, J. Hladík, and J. Novotný, J. Cosmol. Astropart. Phys. 06 (2017) 056.
[17] Z. Stuchlík, D. Charbulák, and J. Schee, Eur. Phys. J. C **78**, 180 (2018).
[18] K. S. Virbhadra, D. Narasimha, and S. M. Chitre, Astron. Astrophys. **337**, 1 (1998).
[19] P. S. Joshi, D. Malafarina, and R. Narayan, Classical Quantum Gravity **28**, 235018 (2011).
[20] P. S. Joshi, D. Malafarina, and R. Narayan, Classical Quantum Gravity **31**, 015002 (2014).
[21] K.-i. Nakao, M. Kimura, M. Patil, and P. S. Joshi, Phys. Rev. D **87**, 104033 (2013).
[22] C. Bambi, L. Modesto, and L. Rachwał, J. Cosmol. Astropart. Phys. 05 (2017) 003.
[23] C. Bambi, Z. Cao, and L. Modesto, Phys. Rev. D **95**, 064006 (2017).
[24] B. Toshmatov, A. Abdujabbarov, Z. Stuchlík, and B. Ahmedov, Phys. Rev. D **91**, 083008 (2015).
[25] B. Toshmatov, C. Bambi, B. Ahmedov, A. Abdujabbarov, and Z. Stuchlík, Eur. Phys. J. C **77**, 542 (2017).
[26] H. Chakrabarty, C. A. Benavides-Gallego, C. Bambi, and L. Modesto, J. High Energy Phys. 3 (2018) 13.
[27] C. Bambi, L. Modesto, S. Porey, and L. Rachwał, Eur. Phys. J. C **78**, 116 (2018).
[28] P. Hořava, J. High Energy Phys. 03 (2009) 020.
[29] P. Hořava and C. M. Melby-Thompson, Phys. Rev. D **82**, 064027 (2010).
[30] P. O. Mazur and E. Mottola, Proc. Natl. Acad. Sci. U.S.A. **101**, 9545 (2004).
[31] C. B. M. H. Chirenti and L. Rezzolla, Classical Quantum Gravity **24**, 4191 (2007).

[32] B. V. Turimov, B. J. Ahmedov, and A. A. Abdujabbarov, Mod. Phys. Lett. A **24**, 733 (2009).
[33] C. Chirenti and L. Rezzolla, Phys. Rev. D **94**, 084016 (2016).
[34] A. A. Abdujabbarov, B. J. Ahmedov, and V. G. Kagramanova, Gen. Relativ. Gravit. **40**, 2515 (2008).
[35] A. Abdujabbarov and B. Ahmedov, Phys. Rev. D **81**, 044022 (2010).
[36] A. Abdujabbarov, B. Ahmedov, and A. Hakimov, Phys. Rev. D **83**, 044053 (2011).
[37] A. A. Abdujabbarov, A. A. Tursunov, B. J. Ahmedov, and A. Kuvatov, Astrophys. Space Sci. **343**, 173 (2013).
[38] A. A. Abdujabbarov, B. J. Ahmedov, and N. B. Jurayeva, Phys. Rev. D **87**, 064042 (2013).
[39] A. Abdujabbarov, B. Ahmedov, O. Rahimov, and U. Salikhbaev, Phys. Scr. **89**, 084008 (2014).
[40] A. Tripathi, J. Yan, Y. Yang, Y. Yan, M. Garnham, Y. Yao, S. Li, Z. Ding, A. B. Abdikamalov, D. Ayzenberg, C. Bambi, T. Dauser, J. A. Garcia, J. Jiang, and S. Nampalliwar, Astrophys. J. **874**, 135 (2019).
[41] C. Bambi, J. Jiang, and J. F. Steiner, Classical Quantum Gravity **33**, 064001 (2016).
[42] Z. Cao, S. Nampalliwar, C. Bambi, T. Dauser, and J. A. García, Phys. Rev. Lett. **120**, 051101 (2018).
[43] L. Kong, Z. Li, and C. Bambi, Astrophys. J. **797**, 78 (2014).
[44] C. Bambi, *Black Holes: A Laboratory for Testing Strong Gravity* (Springer, Singapore, 2017).
[45] Z. Stuchlík, J. Schee, and A. Abdujabbarov, Phys. Rev. D **89**, 104048 (2014).
[46] V. P. Frolov and A. A. Shoom, Phys. Rev. D **82**, 084034 (2010).
[47] V. P. Frolov, Phys. Rev. D **85**, 024020 (2012).
[48] V. Karas, J. Kovar, O. Kopacek, Y. Kojima, P. Slany, and Z. Stuchlik, in *American Astronomical Society Meeting Abstracts* (2012), Vol. 220, p. 430.07.
[49] Z. Stuchlík and M. Kološ, Eur. Phys. J. C **76**, 32 (2016).
[50] J. Kovář, O. Kopáček, V. Karas, and Z. Stuchlík, Classical Quantum Gravity **27**, 135006 (2010).
[51] J. Kovář, P. Slaný, C. Cremaschini, Z. Stuchlík, V. Karas, and A. Trova, Phys. Rev. D **90**, 044029 (2014).
[52] A. Tursunov, Z. Stuchlík, and M. Kološ, Phys. Rev. D **93**, 084012 (2016).
[53] M. Kološ, A. Tursunov, and Z. Stuchlík, Eur. Phys. J. C. **77**, 860 (2017).
[54] J. Bardeen, in *Proceedings of GR5, Tbilisi, USSR*, edited by C. DeWitt and B. DeWitt (Gordon and Breach, New York, 1968), p. 174.
[55] E. Ayón-Beato and A. García, Phys. Rev. Lett. **80**, 5056 (1998).
[56] K. A. Bronnikov, Phys. Rev. D **63**, 044005 (2001).
[57] C. Bambi and L. Modesto, Phys. Lett. B **721**, 329 (2013).
[58] B. Toshmatov, B. Ahmedov, A. Abdujabbarov, and Z. Stuchlík, Phys. Rev. D **89**, 104017 (2014).
[59] Z. Stuchlík and J. Schee, Int. J. Mod. Phys. D **24**, 1550020 (2015).
[60] J. Schee and Z. Stuchlík, J. Cosmol. Astropart. Phys. 06 (2015) 048.
[61] B. Toshmatov, Z. Stuchlík, and B. Ahmedov, Phys. Rev. D **95**, 084037 (2017).
[62] Z.-Y. Fan and X. Wang, Phys. Rev. D **94**, 124027 (2016).
[63] B. Toshmatov, Z. Stuchlík, and B. Ahmedov, Phys. Rev. D **98**, 028501 (2018).
[64] K. A. Bronnikov, Phys. Rev. D **96**, 128501 (2017).
[65] J. Schee and Z. Stuchlík, Astrophys. J. **874**, 12 (2019).
[66] J. Schee and Z. Stuchlík, Eur. Phys. J. C **79**, 988 (2019).
[67] Z. Stuchlík, J. Schee, and D. Ovchinnikov, Astrophys. J. **887**, 145 (2019).
[68] J. Rayimbaev, M. Figueroa, Z. Stuchlík, and B. Juraev, Phys. Rev. D **101**, 104045 (2020).
[69] J. Vrba, A. Abdujabbarov, A. Tursunov, B. Ahmedov, and Z. Stuchlík, Eur. Phys. J. C **79**, 778 (2019).
[70] G. Török, M. A. Abramowicz, W. Kluźniak, and Z. Stuchlík, Astron. Astrophys. **436**, 1 (2005).
[71] G. Török, A. Kotrlová, E. Šrámková, and Z. Stuchlík, Astron. Astrophys. **531**, A59 (2011).
[72] Z. Stuchlík, A. Kotrlová, and G. Török, Astron. Astrophys. **552**, A10 (2013).
[73] Z. Stuchlík and M. Kološ, Mon. Not. R. Astron. Soc **451**, 2575 (2015).
[74] Z. Stuchlík and M. Kološ, Astron. Astrophys. **586**, A130 (2016).
[75] Z. Stuchlík and M. Kološ, Astrophys. J. **825**, 13 (2016).
[76] L. Rezzolla, S. Yoshida, T. J. Maccarone, and O. Zanotti, Mon. Not. R. Astron. Soc **344**, L37 (2003).
[77] A. Kotrlová, G. Török, E. Šrámková, and Z. Stuchlík, Astron. Astrophys. **572**, A79 (2014).
[78] R. Pánis, M. Kološ, and Z. Stuchlík, Eur. Phys. J. C **79**, 479 (2019).
[79] Z. Stuchlík, M. Kološ, J. Kovář, P. Slaný, and A. Tursunov, Universe **6**, 26 (2020).
[80] Z. Stuchlík and M. Kološ, J. Cosmol. Astropart. Phys. 10 (2012) 008.
[81] R. M. Wald, Phys. Rev. D **10**, 1680 (1974).
[82] A. N. Aliev, D. V. Galtsov, and V. I. Petukhov, Astrophys. Space Sci. **124**, 137 (1986).
[83] A. N. Aliev and D. V. Gal'tsov, Sov. Phys. Usp. **32**, 75 (1989).
[84] A. N. Aliev and N. Özdemir, Mon. Not. R. Astron. Soc. **336**, 241 (2002).
[85] J. Kovář, Z. Stuchlík, and V. Karas, Classical Quantum Gravity **25**, 095011 (2008).
[86] O. Kopáček, V. Karas, J. Kovář, and Z. Stuchlík, Astrophys. J. **722**, 1240 (2010).
[87] V. P. Frolov and P. Krtouš, Phys. Rev. D **83**, 024016 (2011).
[88] C. A. Benavides-Gallego, A. Abdujabbarov, D. Malafarina, B. Ahmedov, and C. Bambi, Phys. Rev. D **99**, 044012 (2019).
[89] S. Shaymatov, B. Ahmedov, Z. Stuchlík, and A. Abdujabbarov, Int. J. Mod. Phys. D **27**, 1850088 (2018).
[90] T. Oteev, A. Abdujabbarov, Z. Stuchlík, and B. Ahmedov, Astrophys. Space Sci. **361**, 269 (2016).
[91] B. Toshmatov, A. Abdujabbarov, B. Ahmedov, and Z. Stuchlík, Astrophys. Space Sci. **360**, 19 (2015).
[92] A. A. Abdujabbarov, B. J. Ahmedov, S. R. Shaymatov, and A. S. Rakhmatov, Astrophys. Space Sci. **334**, 237 (2011).
[93] J. R. Rayimbaev, Astrophys. Space Sci. **361**, 288 (2016).
[94] O. G. Rahimov, A. A. Abdujabbarov, and B. J. Ahmedov, Astrophys. Space Sci. **335**, 499 (2011).

[95] O. G. Rahimov, Mod. Phys. Lett. A **26**, 399 (2011).
[96] N. Bakhtiyor, R. Javlon, A. Ahmadjon, and B. Cosimo, arXiv:2005.04752.
[97] R. Javlon, T. Bobur, M. Figueroa, P. Satimbay, and R. Azamkhan, Mod. Phys. Lett. A **35**, 2050056 (2020).
[98] J. R. Rayimbaev, B. J. Ahmedov, N. B. Juraeva, and A. S. Rakhmatov, Astrophys. Space Sci. **356**, 301 (2015).
[99] J. Rayimbaev, B. Turimov, and B. Ahmedov, Int. J. Mod. Phys. D **28**, 1950128 (2019).
[100] F. de Felice and F. Sorge, Classical Quantum Gravity **20**, 469 (2003).
[101] F. de Felice, F. Sorge, and S. Zilio, Classical Quantum Gravity **21**, 961 (2004).
[102] K. Haydarov, A. Abdujabbarov, J. Rayimbaev, and B. Ahmedov, Universe **6**, 44 (2020).
[103] K. Haydarov, J. Rayimbaev, A. Abdujabbarov, S. Palvanov, and D. Begmatova, Eur. Phys. J. C **80**, 399 (2020).
[104] J. Rayimbaev, A. Abdujabbarov, B. Turimov, and F. Atamurotov, arXiv:2004.10031.
[105] M. De Laurentis, Z. Younsi, O. Porth, Y. Mizuno, and L. Rezzolla, Phys. Rev. D **97**, 104024 (2018).
[106] B. Toshmatov, Z. Stuchlík, J. Schee, and B. Ahmedov, Phys. Rev. D **97**, 084058 (2018).
[107] B. Toshmatov, Z. Stuchlík, B. Ahmedov, and D. Malafarina, Phys. Rev. D **99**, 064043 (2019).
[108] Z. Stuchlík and J. Schee, Eur. Phys. J. C **79**, 44 (2019).
[109] M. Kološ, Z. Stuchlík, and A. Tursunov, Classical Quantum Gravity **32**, 165009 (2015).
[110] J. E. McClintock, R. Narayan, S. W. Davis, L. Gou, A. Kulkarni, J. A. Orosz, R. F. Penna, R. A. Remillard, and J. F. Steiner, Classical Quantum Gravity **28**, 114009 (2011).
[111] J. M. Bardeen, W. H. Press, and S. A. Teukolsky, Astrophys. J. **178**, 347 (1972).
[112] K. Mori *et al.*, Astron. J. Lett. **770**, L23 (2013).